

# Gridless Parameter Estimation in Partly Calibrated Rectangular Arrays

Tianyi Liu, Sai Pavan Deram, Khaled Ardah, Martin Haardt, Marc E. Pfetsch, and Marius Pesavento

**Abstract**—Spatial frequency estimation from a mixture of noisy sinusoids finds applications in various fields. While subspace-based methods offer cost-effective super-resolution parameter estimation, they demand precise array calibration, posing challenges for large antennas. In contrast, sparsity-based approaches outperform subspace methods, especially in scenarios with limited snapshots or correlated sources. This study focuses on direction-of-arrival (DOA) estimation using a partly calibrated rectangular array with fully calibrated subarrays. A gridless sparse formulation leveraging shift invariances in the array is developed, yielding two competitive algorithms under the alternating direction method of multipliers (ADMM) and successive convex approximation frameworks, respectively. Numerical simulations show the superior error performance of our proposed method, particularly in highly correlated scenarios, compared to the conventional subspace-based methods. It is demonstrated that the proposed formulation can also be adopted in the fully calibrated case to improve the robustness of the subspace-based methods to the source correlation. Furthermore, we provide a generalization of the proposed method to a more challenging case where a part of the sensors is unobservable due to failures.

**Index Terms**—Gridless DOA estimation, multi-dimensional harmonic retrieval, joint sparsity, multiple measurement vectors, partly calibrated arrays, shift-invariance, ADMM

## I. INTRODUCTION

**D**IRECTION-OF-ARRIVAL (DOA) estimation methods like MUSIC [1] and ESPRIT [2], [3] are recognized for their sensitivity to fluctuations and uncertainties in the array geometry [4] and necessitate an accurate array calibration [5]. As arrays grow larger, calibration becomes increasingly challenging. Partly calibrated arrays (PCAs) have been introduced to address this issue, involving the division of the array into fully calibrated subarrays with uncertain phase relations between them [6], [7].

Recently, several DOA estimation methods for PCAs have been developed [2], [7]–[9]. Search-free subspace-based methods, such as ESPRIT [2], RARE [7], [10] and the algorithm proposed in [11], can be employed for PCAs with identical subarrays. Several above methods have also been extended to PCAs with arbitrary subarray geometries in a search-based manner [8], [9]. For example, a spectral search-based

extension of RARE is proposed in [9]. However, subspace-based methods typically suffer from performance degradation in difficult scenarios, e.g., in the cases with highly correlated source signals and/or a limited number of measurements. To address those challenges, sparsity-based methods have been explored for PCAs [12], [13]. In [14], the authors employ a grid-based sparse model and estimate DOAs by solving a block- and rank-sparse optimization problem. Whereas grid-based methods may suffer from basis mismatch due to the spectrum discretization, a gridless sparse method, termed shift-invariant SPARROW (SI-SPARROW), is introduced in [15] for PCAs, avoiding the sampling over the field-of-view (FOV). Despite the promising error performance demonstrated by the above sparse methods even in challenging scenarios, they both assume a uniform linear subarray structure, limiting DOA estimation to the azimuth direction. The extreme case with only a single snapshot in PCAs is studied in [16], and a novel method that achieves an enhanced angular resolution is proposed by exploiting the approximate orthogonality of the source signals after a transformation.

In this paper, we extend the SI-SPARROW formulation in [15] to the case of a partly calibrated rectangular array (PCRA) with fully calibrated subarrays and unknown inter-subarray displacements, which allows DOA estimation in both azimuth and elevation directions. Although, for notational simplicity, the SI-SPARROW formulation is presented for a PCRA of identical subarrays, it can readily be applied to more general array geometries by employing other shift invariances and/or including virtual unobservable sensors as described in Section VI. Given the solution of the SI-SPARROW formulation, a multidimensional ESPRIT-like method based on the simultaneous Schur decomposition [17] is then provided to finally recover and automatically pair the azimuth and elevation DOAs. Numerical simulations demonstrate the robustness of our proposed method with respect to the source correlation, compared to the conventional partly calibrated DOA estimation methods, where the ESPRIT-like methods are performed on the sample covariance matrix. Moreover, in contrast to the SDP reformulation approach in [15], we develop two competitive algorithms under the ADMM framework and the successive convex approximation (SCA) framework, respectively, for the established SI-SPARROW problem. Both proposed algorithms can be parallelized and exhibit a significantly reduced computation time with the increase of the number of snapshots and the array size, compared to the SDP implementation. In practical scenarios, the customized parallel algorithms become indispensable as the SDP implementation is computationally unattainable. In addition, we show by the

Tianyi Liu and Marius Pesavento are with the Technical University of Darmstadt, Darmstadt, Germany (e-mail: {tliu, pesavento}@nt.tu-darmstadt.de). Sai Pavan Deram is with the IMDEA Networks Institute, Madrid, Spain (e-mail: sai.deram@imdea.org). Khaled Ardah is with the Lenovo Research 5G Lab, Lenovo, Germany (e-mail: kardah@lenovo.com). Martin Haardt is with the Communications Research Laboratory, Ilmenau University of Technology, Ilmenau, Germany (e-mail: martin.haardt@tu-ilmenau.de). Marc E. Pfetsch is with the Research Group Optimization, Technical University of Darmstadt, Darmstadt, Germany (e-mail: pfetsch@mathematik.tu-darmstadt.de).

Part of this work is accepted for publication at IEEE ICASSP 2024.

simulations that the SI-SPARROW formulation can also be employed in the fully calibrated case to improve the robustness of the subspace-based methods, e.g., MUSIC, to the source correlation. Furthermore, we provide a generalization of the SI-SPARROW method to a more challenging case where part of the sensors are unobservable due to failure.

The paper is organized as follows. Section II introduces the partly calibrated array signal model and the shift-invariance properties. In Section III, the SI-SPARROW formulation for DOA estimation in a PCRA is established. In Section IV and V, we devise competitive algorithms for the SI-SPARROW problem under the ADMM framework and the SCA framework, respectively. We further provide a generalization of the SI-SPARROW method to the case with unobservable sensors in Section VI. Simulation results are presented in Section VII, followed by concluding remarks in Section VIII.

*Notation:* We use  $x$ ,  $\mathbf{x}$ , and  $\mathbf{X}$  to denote a scalar, column vector, and matrix, respectively. The  $k$ th entry of a vector  $\mathbf{x}$  is denoted by  $x_k$  and the  $(k, l)$ th entry of a matrix  $\mathbf{X}$  is  $x_{k,l}$ . For any  $x \in \mathbb{C}$ ,  $x^*$  denotes its complex conjugate. The sets of  $M \times M$  Hermitian and positive semidefinite (PSD) Hermitian matrices are denoted by  $\mathbb{S}^M$  and  $\mathbb{S}_+^M$ , respectively. The  $M \times M$  identity matrix is denoted by  $\mathbf{I}_M$ , and  $\mathbf{0}$  and  $\mathbf{1}$  represent a zero matrix and all-ones matrix, respectively. The symbols  $(\cdot)^\top$ ,  $(\cdot)^H$ , and  $(\cdot)^{-1}$  denote the transpose, Hermitian transpose, and inverse, respectively. The trace operator is written as  $\text{tr}(\cdot)$  and  $\|\cdot\|_F$  is the Frobenius norm.

For a real-valued function  $f(\mathbf{X})$  with complex arguments  $\mathbf{X} \in \mathbb{C}^{M \times N}$ , the gradient  $\nabla_{\mathbf{X}} f(\mathbf{X})$  with respect to  $\mathbf{X}$  is defined as an  $M \times N$  matrix with the  $(k, l)$ th entry being  $2 \frac{\partial f(\mathbf{X})}{\partial x_{k,l}^*}$  based on the Wirtinger derivative operators  $\frac{\partial}{\partial x}$  and  $\frac{\partial}{\partial x^*}$  [18]. Moreover, the Hessian of a real-valued quadratic function  $f$  with respect to a complex-valued vector  $\mathbf{x} \in \mathbb{C}^N$ , denoted by  $\nabla_{\mathbf{x}}^2 f(\mathbf{x})$ , is defined in a compact form as an  $N \times N$  matrix with the  $(k, l)$ th entry being  $2 \frac{\partial^2 f(\mathbf{x})}{\partial x_k^* \partial x_l}$  such that, for both real and complex arguments, the real-valued quadratic function  $f$  can be written as the quadratic Taylor series at any  $\mathbf{x}^o$  in a unified form  $f(\mathbf{x}) = f(\mathbf{x}^o) + \Re(\Delta \mathbf{x}^H \nabla_{\mathbf{x}} f(\mathbf{x}^o)) + \frac{1}{2} \Delta \mathbf{x}^H \nabla_{\mathbf{x}}^2 f(\mathbf{x}^o) \nabla_{\mathbf{x}}$  with  $\Delta \mathbf{x} = \mathbf{x} - \mathbf{x}^o$ .

## II. SIGNAL MODEL

Consider an  $M_x \times M_y$  PCRA, as shown in Fig. 1, composed of  $P_x \times P_y$  identical subarrays of  $L_x \times L_y$  sensors with  $M_x = P_x L_x$ ,  $M_y = P_y L_y$ . Let  $M = M_x M_y$  be the total number of sensors in the PCRA. The *unknown* intersubarray displacement between the first and the  $p$ th subarray along the  $x$ -axis (resp.,  $y$ -axis) is denoted by  $\Delta_p^x$  (resp.,  $\Delta_p^y$ ), while  $\delta_l^x$  (resp.,  $\delta_l^y$ ) is the *known* relative position of the  $l$ th sensor in the  $x$ -axis (resp.,  $y$ -axis) within each subarray. Additionally, we assume that  $N_S$  narrowband far-field source signals impinge from distinct unknown DOAs with different azimuth and elevation angles, denoted by  $\phi_i \in [-180^\circ, 180^\circ]$  and  $\theta_i \in [0^\circ, 90^\circ]$ , respectively, for  $i = 1, \dots, N_S$ . Each direction  $(\phi_i, \theta_i)$  can be equivalently represented by a pair of spatial frequencies in the two dimensions defined as

$$\mu_i^x = \pi \cos(\phi_i) \sin(\theta_i) \quad \text{and} \quad \mu_i^y = \pi \sin(\phi_i) \sin(\theta_i), \quad (1)$$

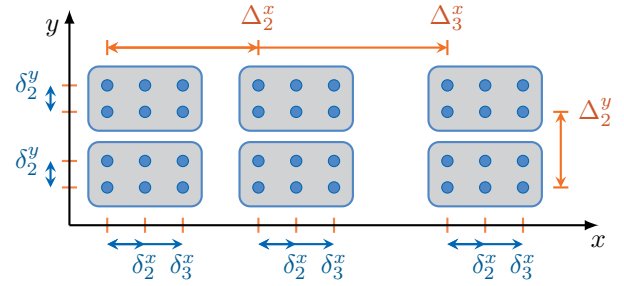


Fig. 1. Example of a PCRA composed of  $3 \times 2$  subarrays with  $3 \times 2$  sensors per subarray.

respectively. The spatial frequencies of the  $N_S$  sources are summarized in  $\boldsymbol{\mu} = [(\boldsymbol{\mu}^x)^\top, (\boldsymbol{\mu}^y)^\top]^\top$  with  $\boldsymbol{\mu}^x = [\mu_1^x, \dots, \mu_{N_S}^x]^\top$  and  $\boldsymbol{\mu}^y = [\mu_1^y, \dots, \mu_{N_S}^y]^\top$ . Let  $\mathbf{Y} \in \mathbb{C}^{M \times N}$  be the measurement matrix where the  $(m, n)$ th entry  $y_{mn}$  is the output at sensor  $m$  in time-slot  $n$ . The measurement matrix is modeled as

$$\mathbf{Y} = \mathbf{A}(\boldsymbol{\mu})\boldsymbol{\Psi} + \mathbf{N}, \quad (2)$$

where the matrix  $\boldsymbol{\Psi} \in \mathbb{C}^{N_S \times N}$  contains the source waveforms with  $\psi_{i,n}$  being the waveform from source  $i$  at time instant  $n$ . The matrix  $\mathbf{N} \in \mathbb{C}^{M \times N}$  comprises noise entries independently and identically distributed according to  $\mathcal{CN}(0, \sigma_n^2)$ . Furthermore,  $\mathbf{A}(\boldsymbol{\mu}^x, \boldsymbol{\mu}^y) \in \mathbb{C}^{M \times N_S}$  is the matrix collecting the  $N_S$  steering vectors of the 2D array as

$$\mathbf{A}(\boldsymbol{\mu}) = [\mathbf{a}(\mu_1^x, \mu_1^y) \quad \dots \quad \mathbf{a}(\mu_{N_S}^x, \mu_{N_S}^y)], \quad (3)$$

where  $\mathbf{a}(\mu_i^x, \mu_i^y) \in \mathbb{C}^M$  is the array-dependent steering vector in the direction of source  $i$ . For the considered PCRA, the array steering vector in the direction  $(\mu^x, \mu^y)$  is expressed as

$$\mathbf{a}(\mu^x, \mu^y) = \mathbf{a}_x(\mu^x) \otimes \mathbf{a}_y(\mu^y), \quad (4)$$

where  $\mathbf{a}_x(\mu^x) \in \mathbb{C}^{M_x}$  and  $\mathbf{a}_y(\mu^y) \in \mathbb{C}^{M_y}$  are defined as

$$\begin{aligned} \mathbf{a}_x(\mu^x) &= [1, \dots, e^{j\mu^x \delta_{L_x}^x}, e^{j\mu^x \Delta_2^x}, \dots, e^{j\mu^x (\Delta_{P_x}^x + \delta_{L_x}^x)}]^\top, \\ \mathbf{a}_y(\mu^y) &= [1, \dots, e^{j\mu^y \delta_{L_y}^y}, e^{j\mu^y \Delta_2^y}, \dots, e^{j\mu^y (\Delta_{P_y}^y + \delta_{L_y}^y)}]^\top. \end{aligned}$$

In other words, the steering vector contains the sensor responses sorted by vectorizing the 2D array along the  $y$ -axis.

In the following, we introduce the shift-invariance properties of the array. Toward this goal, we define the selection matrices

$$\mathbf{J}_p^x = \mathbf{e}_{P_x, p} \otimes \mathbf{I}_{L_x} \otimes \mathbf{I}_{P_y} \otimes \mathbf{I}_{L_y}, \quad p = 1, \dots, P_x, \quad (5a)$$

$$\mathbf{K}_l^x = \mathbf{I}_{P_x} \otimes \mathbf{e}_{L_x, l} \otimes \mathbf{I}_{P_y} \otimes \mathbf{I}_{L_y}, \quad l = 1, \dots, L_x, \quad (5b)$$

$$\mathbf{J}_p^y = \mathbf{I}_{P_x} \otimes \mathbf{I}_{L_x} \otimes \mathbf{e}_{P_y, p} \otimes \mathbf{I}_{L_y}, \quad p = 1, \dots, P_y, \quad (5c)$$

$$\mathbf{K}_l^y = \mathbf{I}_{P_x} \otimes \mathbf{I}_{L_x} \otimes \mathbf{I}_{P_y} \otimes \mathbf{e}_{L_y, l}, \quad l = 1, \dots, L_y, \quad (5d)$$

to assign sensors to various shift-invariant groups, where  $\mathbf{e}_{P,p} = [0, \dots, 0, 1, 0, \dots, 0]^\top$  is the  $P$ -dimensional basis vector with the  $p$ th entry being one and all the other entries being zero. As depicted in Fig. 2, by the operation  $\mathbf{J}_p^x \mathbf{a}$  (resp.,  $\mathbf{J}_p^y \mathbf{a}$ ), the responses of all subarrays at the  $p$ th position in the  $x$ -axis (resp.,  $y$ -axis) are selected. Similarly,  $\mathbf{K}_l^x$  and  $\mathbf{K}_l^y$  are used to select all sensors at the  $l$ th position in the  $x$ -axis and  $y$ -axis, respectively, within the subarrays. Then the shift-invariance properties of the steering matrix are given as

$$(\mathbf{J}_p^x)^\top \mathbf{A}(\boldsymbol{\mu}) = (\mathbf{J}_1^x)^\top \mathbf{A}(\boldsymbol{\mu}) \boldsymbol{\Phi}(\Delta_p^x \boldsymbol{\mu}^x), \quad p = 2, \dots, P_x, \quad (6a)$$

$$(\mathbf{K}_l^x)^\top \mathbf{A}(\boldsymbol{\mu}) = (\mathbf{K}_1^x)^\top \mathbf{A}(\boldsymbol{\mu}) \boldsymbol{\Phi}(\delta_l^x \boldsymbol{\mu}^x), \quad l = 2, \dots, L_x, \quad (6b)$$

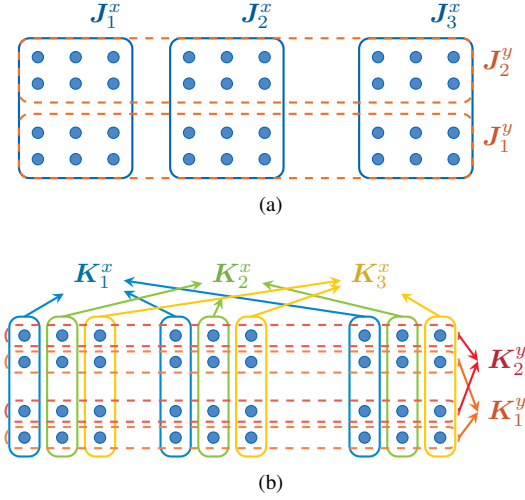


Fig. 2. Different shift-invariant groups for the PCRA in Fig. 1: The shift-invariant groups that involve the intersubarray displacements are indicated in (a), whereas the shift-invariant groups that involve the intrasubarray displacements are indicated in (b).

$$(\mathbf{J}_p^y)^T \mathbf{A}(\boldsymbol{\mu}) = (\mathbf{J}_1^y)^T \mathbf{A}(\boldsymbol{\mu}) \Phi(\Delta_p^y \boldsymbol{\mu}^y), \quad p=2, \dots, P_y, \quad (6c)$$

$$(\mathbf{K}_l^y)^T \mathbf{A}(\boldsymbol{\mu}) = (\mathbf{K}_1^y)^T \mathbf{A}(\boldsymbol{\mu}) \Phi(\delta_l^y \boldsymbol{\mu}^y), \quad l=2, \dots, L_y, \quad (6d)$$

where  $\Phi(\mathbf{x}) = \text{Diag}(e^{jx_1}, \dots, e^{jx_N}) \in \mathbb{C}^{N \times N}$  for a vector  $\mathbf{x} \in \mathbb{R}^N$ . Also, it is straightforward to see that each single sensor forms a shift-invariant group regardless of the array configuration, and this shift-invariance property is written as

$$\mathbf{e}_{M,m}^T \mathbf{A}(\boldsymbol{\mu}) = \mathbf{e}_{M,1}^T \mathbf{A}(\boldsymbol{\mu}) \Phi((\Delta_p^x + \delta_k^x) \boldsymbol{\mu}^x) \Phi((\Delta_q^y + \delta_l^y) \boldsymbol{\mu}^y) \quad (7)$$

for  $p = 1, \dots, P_x$ ,  $q = 1, \dots, P_y$ ,  $k = 1, \dots, L_x$ ,  $l = 1, \dots, L_y$  and  $m = ((p-1)L_x + (k-1))M_y + (q-1)L_y + l$ . Additional shift invariances can be exploited if other array topologies are given, such as shift-invariances with overlapping groups or centro-symmetry. For simplicity, in this paper, we limit our discussion to the example of the PCRA in Fig. (1). Furthermore, we remark that the shift-invariance properties in (6) and (7) can naturally be applied to a steering matrix constructed according to (3) with any set of frequencies  $\boldsymbol{\mu}$ .

*Remark 1:* Since the sensor displacements  $\delta_l^x$  and  $\delta_l^y$  are known, the shift-invariance equations in (6b) and (6d) can be used to estimate the spatial frequencies  $\boldsymbol{\mu}$  by the 2D-ESPRIT methods in [17], [19], [20], with automatic pairing.

### III. SPARSE SIGNAL FORMULATION

This section begins with an introduction to an equivalent sparse representation of the measurement model in (2) obtained by sampling the FOV and the state-of-the-art SPARROW formulation [13] constructed on the grid-based sparse model. To address the challenge that the intersubarray displacements are unknown, a gridless relaxation of the SPARROW formulation is proposed by using the shift-invariance properties in (6) of the considered array.

#### A. Grid-Based Sparse Formulation for Fully Calibrated Arrays

In the following, the classic grid-based sparse formulation for the DOA estimation problem is introduced. This formu-

lation requires the full calibration information and does not exploit any shift-invariance properties in the array.

We define a sparse representation for the model in (2) as

$$\mathbf{Y} = \mathbf{A}(\boldsymbol{\nu})\mathbf{X} + \mathbf{N}, \quad (8)$$

where  $\mathbf{A}(\boldsymbol{\nu}) \in \mathbb{C}^{M \times K}$  is an overcomplete dictionary constructed according to (3) by sampling the field-of-view in  $K \gg N_S$  directions with spatial frequencies  $\boldsymbol{\nu} = [(\boldsymbol{\nu}^x)^T, (\boldsymbol{\nu}^y)^T]^T$ , where  $\boldsymbol{\nu}^x = [\nu_1^x, \dots, \nu_K^x]^T$  and  $\boldsymbol{\nu}^y = [\nu_1^y, \dots, \nu_K^y]^T$ , and  $\mathbf{X} \in \mathbb{C}^{K \times N}$  is designed to be a sparse representation of the waveform matrix  $\boldsymbol{\Psi}$ . Specifically, provided that the true frequencies  $\boldsymbol{\mu}$  are contained in the frequency grid, i.e.,

$$\{(\mu_i^x, \mu_i^y)\}_{i=1}^{N_S} \subset \{(\nu_k^x, \nu_k^y)\}_{k=1}^K, \quad (9)$$

then  $\mathbf{X} = [\mathbf{x}_1, \dots, \mathbf{x}_K]^T$  admits a row-sparse structure, which has only  $N_S$  nonzero rows  $\mathbf{x}_k^T$  corresponding to the waveforms of the  $N_S$  sources. For simplicity, in the rest of the paper, the dictionary is referred to as  $\mathbf{A} = \mathbf{A}(\boldsymbol{\nu})$ . Based on the sparse model in (8), the DOA estimation problem can be formulated as the well-known convex mixed-norm minimization

$$\min_{\mathbf{X} \in \mathbb{C}^{K \times N}} \frac{1}{2} \|\mathbf{Y} - \mathbf{A}\mathbf{X}\|_F^2 + \lambda \sqrt{N} \|\mathbf{X}\|_{2,1}, \quad (10)$$

where  $\lambda > 0$  is the regularization parameter and

$$\|\mathbf{X}\|_{2,1} = \sum_{k=1}^K \|\mathbf{x}_k\|_2$$

is the  $\ell_{2,1}$ -norm. Since we are only interested in recovering the DOAs, the mixed-norm minimization problem (10) can be equivalently reformulated as the SPARROW problem [13]

$$\min_{\mathbf{S} \in \mathbb{D}_+^K} \text{tr}((\mathbf{A}\mathbf{S}\mathbf{A}^H + \lambda \mathbf{I}_M)^{-1} \widehat{\mathbf{R}}) + \text{tr}(\mathbf{S}) \quad (11)$$

with the sample covariance matrix  $\widehat{\mathbf{R}} = \mathbf{Y}\mathbf{Y}^H/N$ . The solutions  $\widehat{\mathbf{X}}$  and  $\widehat{\mathbf{S}}$  of problems (10) and (11), respectively, are related by

$$\widehat{\mathbf{S}} = \frac{1}{\sqrt{N}} \text{Diag}(\|\widehat{\mathbf{x}}_1\|_2, \dots, \|\widehat{\mathbf{x}}_K\|_2).$$

Compared to problem (10), problem (11) has a reduced variable size and the DOAs are equivalently indicated by the nonzero diagonal entries of  $\mathbf{S}$ . Problem (11) can be further reformulated as a semidefinite program (SDP), which can be solved by a generic solver based on interior-point methods, e.g., MOSEK [21]. Alternatively, a customized algorithm for problem (11) based on coordinate descent is devised in [13], which is more scalable than the SDP implementation in the case of large array sizes.

However, the grid-based formulation (11) has two drawbacks. First, the on-grid assumption (9) is often impractical due to the limited grid size, leading to spectral leakage and basis mismatch [22], [23] in the recovered signal. Second, constructing the dictionary  $\mathbf{A}$  requires complete array calibration, whereas our scenario assumes unknown intersubarray displacements. Therefore, in the following, we develop a gridless approach by relaxing the grid-based SPARROW problem (11).

#### B. Gridless Shift-Invariant Formulation

A straightforward gridless extension of problem (11) is jointly learning a dictionary  $\mathbf{A}$  in the array manifold, i.e.,

$$\min_{\mathbf{S} \in \mathbb{D}_+^K, \mathbf{A} \in \mathcal{A}^K} \text{tr}((\mathbf{A}\mathbf{S}\mathbf{A}^H + \lambda \mathbf{I}_M)^{-1} \widehat{\mathbf{R}}) + \text{tr}(\mathbf{S}), \quad (12)$$

where  $\mathcal{A}^K = \{\mathbf{A}(\boldsymbol{\nu}) \mid \boldsymbol{\nu} \in [-\pi, \pi]^{2K}, (\nu_i^x, \nu_i^y) \neq (\nu_j^x, \nu_j^y) \forall i, j = 1, \dots, K, i \neq j\}$  is the array manifold with  $K$  distinct DOAs. However, Problem (12) cannot be easily solved and the construction of the array manifold still requires complete array calibration. To relax problem (12), we first reformulate it by introducing a slack variable. As the steering vectors contain unit-modulus entries, it holds that

$$\text{tr}(\mathbf{A}\mathbf{S}\mathbf{A}^H) = \sum_{i=1}^M s_{i,i} \sum_{j=1}^M |a_{i,j}|^2 = M \text{tr}(\mathbf{S}).$$

With a slack variable  $\mathbf{Q}$ , problem (12) can be equivalently written as

$$\begin{aligned} \min_{\mathbf{S} \in \mathbb{D}_+^N, \mathbf{A} \in \mathcal{A}^K, \mathbf{Q} \in \mathbb{S}_+^M} M \text{tr}((\mathbf{Q} + \lambda \mathbf{I}_M)^{-1} \widehat{\mathbf{R}}) + \text{tr}(\mathbf{Q}) \quad (13a) \\ \text{s.t. } \mathbf{Q} = \mathbf{A}\mathbf{S}\mathbf{A}^H, \quad (13b) \end{aligned}$$

where  $\mathbb{S}_+^M$  denotes the set of  $M \times M$  positive semidefinite Hermitian matrices. The objective function in the reformulation (13) depends only on variable  $\mathbf{Q}$  whose structure is specified by the dictionary-based constraint (13b). Also, the trace-term  $\text{tr}(\mathbf{Q})$  in (13a) promotes rank-sparsity of  $\mathbf{Q}$  as it is equivalent to the nuclear norm of  $\mathbf{Q}$  for  $\mathbf{Q} \succeq 0$  [24]. From the reformulation (13), one may immediately obtain a simple gridless relaxation by discarding the dictionary-specific structural constraint (13b). This is equivalent to relaxing the array manifold  $\mathcal{A}^K$  to be the complete space  $\mathbb{C}^{M \times K}$ , consequently yielding inferior accuracy on the estimated DOAs.

To improve estimation accuracy, we further introduce several structural constraints on  $\mathbf{Q}$  in place of the dictionary-based constraint (13b), using the shift-invariance properties of elements in  $\mathcal{A}^K$ . Applying the shift-invariance properties in (6) to the dictionary  $\mathbf{A}(\boldsymbol{\nu})$ , we can obtain the following identity:

$$\begin{aligned} (\mathbf{J}_p^x)^\top \mathbf{Q} \mathbf{J}_p^x &= (\mathbf{J}_p^x)^\top \mathbf{A} \mathbf{S} \mathbf{A}^H \mathbf{J}_p^x \\ &= (\mathbf{J}_1^x)^\top \mathbf{A} \Phi(\Delta_p^x \boldsymbol{\nu}^x) \mathbf{S} (\Phi(\Delta_p^x \boldsymbol{\nu}^x))^\top \mathbf{A}^H \mathbf{J}_1^x \\ &= (\mathbf{J}_1^x)^\top \mathbf{A} \mathbf{S} \mathbf{A}^H \mathbf{J}_1^x = (\mathbf{J}_1^x)^\top \mathbf{Q} \mathbf{J}_1^x, \end{aligned}$$

for  $p = 2, \dots, P_x$ . The same identity can be extended to the other shift-invariance groups stated in (6) and (7), which leads to the following set of structural constraints:

$$(\mathbf{J}_p^x)^\top \mathbf{Q} \mathbf{J}_p^x = (\mathbf{J}_1^x)^\top \mathbf{Q} \mathbf{J}_1^x, \quad p = 2, \dots, P_x, \quad (14a)$$

$$(\mathbf{K}_l^x)^\top \mathbf{Q} \mathbf{K}_l^x = (\mathbf{K}_1^x)^\top \mathbf{Q} \mathbf{K}_1^x, \quad l = 2, \dots, L_x, \quad (14b)$$

$$(\mathbf{J}_p^y)^\top \mathbf{Q} \mathbf{J}_p^y = (\mathbf{J}_1^y)^\top \mathbf{Q} \mathbf{J}_1^y, \quad p = 2, \dots, P_y, \quad (14c)$$

$$(\mathbf{K}_l^y)^\top \mathbf{Q} \mathbf{K}_l^y = (\mathbf{K}_1^y)^\top \mathbf{Q} \mathbf{K}_1^y, \quad l = 2, \dots, L_y, \quad (14d)$$

$$q_{ii} = q_{11}, \quad i = 2, \dots, M. \quad (14e)$$

The structural constraints (14) essentially require that, for any pair of shift-invariant sensor groups, the corresponding submatrices in  $\mathbf{Q}$  are identical. Thus, the constraints (14) define a subspace of  $M \times M$  Hermitian matrices, denoted by

$$\mathcal{T}^M = \{\mathbf{Q} \in \mathbb{S}^M \mid \mathbf{Q} \text{ satisfies the constraints in (14)}\}. \quad (15)$$

Let  $f(\mathbf{Q})$  denote the objective function in (13a), i.e.,

$$f(\mathbf{Q}) = M \text{tr}((\mathbf{Q} + \lambda \mathbf{I}_M)^{-1} \widehat{\mathbf{R}}) + \text{tr}(\mathbf{Q}). \quad (16)$$

Replacing the dictionary-based constraint (13b) by the structural constraints (14) leads to the following gridless shift-invariant SPARROW (SI-SPARROW) problem:

$$\min_{\mathbf{Q} \in \mathbb{S}_+^M \cap \mathcal{T}^M} f(\mathbf{Q}). \quad (17)$$

In the original problem (13),  $\mathbf{Q}$  is designed to span the same

subspace as the corresponding steering matrix  $\mathbf{A}$ . Hence, the solution  $\widehat{\mathbf{Q}}$  of problem (17) can effectively substitute the sample covariance matrix  $\widehat{\mathbf{R}}$  in the 2D-ESPRIT mentioned in Remark 1 in Section II to estimate the spatial frequencies in a search-free manner.

Furthermore, in the special case where the subarrays and the sensors within each subarray are uniformly placed in the two dimensions, respectively, additional shift invariances can be used and this leads to a multilevel Toeplitz structural constraint on  $\mathbf{Q}$ . In this case, when the rank  $r$  of solution  $\widehat{\mathbf{Q}}$  is sufficiently low,  $\widehat{\mathbf{Q}}$  can be uniquely factorized to the form in (13b) with  $r$  distinct DOAs, which is known as Vandermonde decomposition. Some sufficient conditions for the existence of the Vandermonde decomposition of multilevel Toeplitz matrices and a constructive method for finding the decomposition are provided in [25]. For simplicity, the SI-SPARROW problem in (17) is formulated for a PCRA with identical subarrays. However, our proposed method is not restricted to a specific array geometry since a problem formulation similar to (17) can be readily obtained for more general array geometries by reconstructing the shift-invariant subspace  $\mathcal{T}^M$  in (15) based on the shift invariances in the given array.

Similar to the grid-based formulation in (11), problem (17) can be equivalently written as a SDP problem

$$\begin{aligned} \min_{\mathbf{Q} \in \mathbb{S}_+^M \cap \mathcal{T}^M, \mathbf{T}_N \in \mathbb{S}_+^N} \frac{M}{N} \text{tr}(\mathbf{T}_N) + \text{tr}(\mathbf{Q}) \quad (18a) \\ \text{s.t. } \begin{bmatrix} \mathbf{T}_N & \mathbf{Y}^H \\ \mathbf{Y} & \mathbf{Q} + \lambda \mathbf{I}_M \end{bmatrix} \succeq 0 \quad (18b) \end{aligned}$$

by using the reformulation technique in [13] and solved by an interior-point solver. Note that the positive semidefiniteness of  $\mathbf{T}_N$  is enforced by the PSD constraint (18b). In [13], the authors also present an alternative SDP reformulation

$$\begin{aligned} \min_{\mathbf{Q} \in \mathbb{S}_+^M \cap \mathcal{T}^M, \mathbf{T}_M \in \mathbb{S}_+^M} M \text{tr}(\mathbf{T}_M \widehat{\mathbf{R}}) + \text{tr}(\mathbf{Q}) \quad (19) \\ \text{s.t. } \begin{bmatrix} \mathbf{T}_M & \mathbf{I}_M \\ \mathbf{I}_M & \mathbf{Q} + \lambda \mathbf{I}_M \end{bmatrix} \succeq 0, \end{aligned}$$

where the dimension of the semidefinite matrix constraint depends only on the number of sensors  $M$ . Hence, problem formulation (19) is preferable for the oversampled case, i.e.,  $N > M$ , and (18) is preferable otherwise. However, as demonstrated in the numerical results in Section VII, the above SDP implementations become computationally intractable in the case with a large number of sensors  $M$ , due to the large dimension of the semidefinite matrix constraints. Hence, inspired by the coordinate descent implementation in [13] for the grid-based SPARROW (11), we develop in the following section an efficient iterative algorithm for solving the SI-SPARROW problem (17) under the ADMM algorithmic framework.

### C. Alternative Expression for Shift-Invariant Subspace

Before presenting the algorithms for solving (17), we first introduce an alternative expression for the elements of the shift-invariant subspace  $\mathcal{T}^M$ . The structural constraints (14) essentially require the identity between the submatrices in  $\mathbf{Q}$  corresponding to any pair of shift-invariant sensor groups. This means that any matrix  $\mathbf{Q} \in \mathcal{T}^M$  can be equivalently expressed by introducing a reduced set of independent variables. For a

matrix  $\mathbf{Q} \in \mathcal{T}^M$ , let  $\mathbf{q} = [q_1, \dots, q_I]^T \in \mathbb{C}^I$  be a vector that contains all the  $I$  independent variables in the upper triangle of  $\mathbf{Q}$  such that each entry of  $\mathbf{Q}$  contains either one variable in  $\mathbf{q}$  or its complex conjugate. In particular, let  $q_1$  be the independent variable on the main diagonal of  $\mathbf{Q}$ , which is real-valued since  $\mathbf{Q}$  is Hermitian. Furthermore, define

$$\Omega_i = \frac{\partial \mathbf{Q}}{\partial q_i} \in \{0, 1\}^{M \times M}, \quad \text{for } i = 1, \dots, I, \quad (20)$$

as the indicator matrix for the independent variable  $q_i$ . The matrix  $\Omega_i$  has a one in the entries of  $\mathbf{Q}$  occupied by  $q_i$  and a zero elsewhere. The entries of  $\mathbf{Q}$  occupied by the complex conjugate of  $q_i$  are then indicated by  $\Omega_i^T$  for  $i = 2, \dots, I$ . In summary, any matrix  $\mathbf{Q} \in \mathcal{T}^M$  can be expressed as

$$\mathbf{Q} = q_1 \Omega_1 + \sum_{i=2}^I (q_i \Omega_i + q_i^* \Omega_i^T) \quad \text{with } q_1 \in \mathbb{R} \text{ and } q_i \in \mathbb{C}, \quad i = 2, \dots, I. \quad (21)$$

Based on the expression in (21), the function  $f$ , in the subspace  $\mathcal{T}^M$ , can be regarded as a function dependent only on  $\mathbf{q}$ . Hence, the notations  $f(\mathbf{Q})$  and  $f(\mathbf{q})$  are used interchangeably in this paper when only elements of  $\mathcal{T}^M$  are considered.

#### D. Multi-Invariance Multidimensional ESPRIT

As mentioned in Remark 1 in Section II, the shift-invariance equations in (6b) and (6d) with the known sensor displacements  $\delta_l^x$  and  $\delta_l^y$  within each subarray can be used to estimate the spatial frequencies by the multidimensional ESPRIT (MD-ESPRIT) method that is implemented by the simultaneous diagonalization or Schur decomposition [19], [26]. Similar to the conventional approach where the MD-ESPRIT method is performed on the sample covariance matrix  $\hat{\mathbf{R}}$ , the MD-ESPRIT method can be employed to further recover the spatial frequencies from the matrix  $\hat{\mathbf{Q}}$  reconstructed by the proposed SI-SPARROW formulation in (17).

However, the MD-ESPRIT method can only consider a single shift-invariance equation in each dimension. To utilize all the shift-invariance equations in (6b) and (6d) that involve the known sensor displacements  $\delta_l^x$  for  $l = 2, \dots, L_x$  and  $\delta_l^y$  for  $l = 2, \dots, L_y$ , we extend the MD-ESPRIT method by performing the following two steps. First, the original MD-ESPRIT method is applied to an approximate problem where each shift-invariance equation is considered to be a virtual dimension. Specifically, the diagonal matrices  $\Phi(\delta_l^x \boldsymbol{\mu}^x)$  and  $\Phi(\delta_k^x \boldsymbol{\mu}^x)$  (resp.,  $\Phi(\delta_l^y \boldsymbol{\mu}^y)$  and  $\Phi(\delta_k^y \boldsymbol{\mu}^y)$ ) in two different equations in (6), i.e.,  $l \neq k$ , are treated as independent. The MD-ESPRIT method recovers the diagonal matrices

$$\Phi(\delta_l^x \boldsymbol{\mu}^x) = \text{Diag}(e^{j\mu_1^x \delta_l^x}, \dots, e^{j\mu_{N_s}^x \delta_l^x}), \quad l = 2, \dots, L_x, \quad (22)$$

$$\Phi(\delta_l^y \boldsymbol{\mu}^y) = \text{Diag}(e^{j\mu_1^y \delta_l^y}, \dots, e^{j\mu_{N_s}^y \delta_l^y}), \quad l = 2, \dots, L_y.$$

The entries of the recovered diagonal matrices in (22) can be used to reconstruct the 1D subarray steering vectors corresponding to each frequency to be estimated, defined as

$$\begin{aligned} \mathbf{v}^x(\mu_i^x) &= [1, e^{j\mu_i^x \delta_2^x}, \dots, e^{j\mu_i^x \delta_{L_x}^x}]^T, \\ \mathbf{v}^y(\mu_i^y) &= [1, e^{j\mu_i^y \delta_2^y}, \dots, e^{j\mu_i^y \delta_{L_y}^y}]^T, \end{aligned} \quad (23)$$

for  $i = 1, \dots, N_s$ . Then, with the known sensors displacements  $\delta_l^x$  and  $\delta_l^y$  within each subarray, the recovery of the frequencies can be performed independently from each reconstructed 1D steering vector in (23) by a single-source

---

#### Algorithm 1: ADMM Algorithm for SI-SPARROW.

---

**Input:** Sample covariance matrix  $\hat{\mathbf{R}}$ , indicator matrices  $\{\Omega_i\}_i^I$ , regularization parameter  $\lambda > 0$ , tolerances  $\varepsilon^{\text{abs}}, \varepsilon^{\text{rel}} > 0$

- 1 Initialize  $\mathbf{Q}^{(0)}, \mathbf{Z}^{(0)}, \mathbf{U}^{(0)}, t \leftarrow 0$ ;
- 2 **while not converged do**
- 3     Update  $\mathbf{Q}^{(t)}$  by solving (27a) using Algorithm 2;
- 4      $\mathbf{Z}^{(t+1)} \leftarrow \mathcal{P}_{\mathbb{S}_+^M}(\mathbf{Q}^{(t+1)} + \mathbf{U}^{(t)})$ ;
- 5      $\mathbf{U}^{(t+1)} \leftarrow \mathbf{U}^{(t)} + \mathbf{Q}^{(t+1)} - \mathbf{Z}^{(t+1)}$ ;
- 6      $t \leftarrow t + 1$ ;
- 7 **return**  $\mathbf{Q}^{(t)}$

---

recovery method, e.g., the deterministic maximum likelihood (DML) estimator via a simple 1D grid search in the general case, or the search-free root-MUSIC in the special case where the sensors in each subarray are placed uniformly in each dimension, respectively. Note that, in the single-source case, the DML estimator reduces to the conventional beamformer. The method described above is referred to as multi-invariance multidimensional ESPRIT (MI-MD-ESPRIT) in this paper.

#### IV. ADMM FOR SHIFT-INVARIANT SPARROW

In this section, we use the ADMM algorithmic framework to solve the SI-SPARROW problem (17). The choice of ADMM is motivated by the fact that problem (17) can be easily solved when only one of the two kinds of constraints, i.e., either the PSD constraint or the shift-invariance constraints, needs to be fulfilled. Specifically, the ADMM framework is employed to decompose the problem such that, in each subproblem, only one of the constraints needs to be fulfilled. We assume that the sample covariance matrix  $\hat{\mathbf{R}}$  is positive definite. This assumption is required to ensure the convergence of the solution approach for the primal subproblem in ADMM, which will be introduced later. In the undersampled case, i.e.,  $N < M$ , where the sample covariance matrix is always rank deficient, a small positive diagonal loading onto the sample covariance matrix is performed before solving (17), i.e., replacing  $\hat{\mathbf{R}}$  by  $\hat{\mathbf{R}} + \iota \mathbf{I}_M$  with a small  $\iota > 0$ .

To apply the ADMM framework, we first write problem (17) as the following equivalent formulation:

$$\min_{\mathbf{Q} \in \mathcal{T}^M, \mathbf{Z} \in \mathbb{S}_+^M} f(\mathbf{Q}) + g(\mathbf{Z}) \quad (24a)$$

$$\text{s.t. } \mathbf{Q} - \mathbf{Z} = \mathbf{0} \quad (24b)$$

$$\mathbf{Q} + \lambda \mathbf{I}_M \succ 0, \quad (24c)$$

where  $g$  is the indicator function of the PSD cone  $\mathbb{S}_+^M$ , i.e.,

$$g(\mathbf{Z}) = 0 \text{ for } \mathbf{Z} \in \mathbb{S}_+^M \text{ and } g(\mathbf{Z}) = +\infty \text{ otherwise.} \quad (25)$$

In the reformulation (24), by introducing an auxiliary variable  $\mathbf{Z}$ , the shift-invariance constraints (14) are separated from the PSD constraint  $\mathbf{Q} \succeq 0$  so that the two types of constraints can be addressed alternatively. As a necessary condition of  $\mathbf{Q} = \mathbf{Z} \succeq 0$ , the constraint (24c) is redundant. However, it is required to ensure the convexity of the primal subproblem in ADMM that is introduced in (27a), since  $f$  is convex only in the subset where  $\mathbf{Q} + \lambda \mathbf{I}_M \succ 0$ .

---

**Algorithm 2:** SCA Algorithm for the  $\mathbf{Q}$ -update.
 

---

**Input:**  $\mathbf{Q}$ , indicator matrices  $\{\Omega_i\}_i^L$ ,  $\lambda > 0$ , tolerance  $\eta > 0$

- 1 Initialize  $\mathbf{Q}^{(0)}, l \leftarrow 0$ ;
- 2 **while** not converged **do**
- 3     Compute  $\tilde{\mathbf{q}}^{(l)}$  according to (35) and (36);
- 4     Compute  $\tilde{\mathbf{Q}}^{(l)}$  from  $\tilde{\mathbf{q}}^{(l)}$  according to (21);
- 5     Compute step size  $\alpha^{(l)}$  by Armijo rule described in Section IV-A2;
- 6      $\mathbf{Q}^{(l+1)} \leftarrow \mathbf{Q}^{(l)} + \alpha^{(l)}(\tilde{\mathbf{Q}}^{(l)} - \mathbf{Q}^{(l)})$ ;
- 7      $l \leftarrow l + 1$ ;
- 8 **return**  $\mathbf{Q}^{(l)}$

---

The augmented Lagrangian of problem (24) is [27]

$$L_\rho(\mathbf{Q}, \mathbf{Z}, \mathbf{U}) = f(\mathbf{Q}) + g(\mathbf{Z}) + \frac{\rho}{2} \|\mathbf{Q} - \mathbf{Z} + \mathbf{U}\|_F^2, \quad (26)$$

where  $\rho > 0$  is the penalty parameter and  $\mathbf{U} \in \mathbb{S}^M$  is the dual variable scaled by  $1/\rho$ . Note that  $L_0$  denotes the unaugmented Lagrangian. Let  $\mathbf{Q}^{(t)}, \mathbf{Z}^{(t)}, \mathbf{U}^{(t)}$  be the value of primal and dual variables at iteration  $t$ . The scaled form of ADMM for problem (24) consists of the following steps in each iteration:

$$\begin{aligned} \mathbf{Q}^{(t+1)} &= \underset{\mathbf{Q} \in \mathcal{T}^M}{\operatorname{argmin}} f(\mathbf{Q}) + \frac{\rho}{2} \|\mathbf{Q} - \mathbf{Z}^{(t)} + \mathbf{U}^{(t)}\|_F^2 \\ &\text{s.t. } \mathbf{Q} + \lambda \mathbf{I}_M \succ 0, \end{aligned} \quad (27a)$$

$$\mathbf{Z}^{(t+1)} = \mathcal{P}_{\mathbb{S}_+^M}(\mathbf{Q}^{(t+1)} + \mathbf{U}^{(t)}), \quad (27b)$$

$$\mathbf{U}^{(t+1)} = \mathbf{U}^{(t)} + \mathbf{Q}^{(t+1)} - \mathbf{Z}^{(t+1)}. \quad (27c)$$

The projection onto the PSD cone  $\mathbb{S}_+^M$ , denoted by  $\mathcal{P}_{\mathbb{S}_+^M}$ , can be calculated by discarding the components with negative eigenvalues in the eigenvalue decomposition (EVD) of the argument [28]. The subproblem for the  $\mathbf{Q}$ -update (27a) is convex. Define  $\bar{\mathbf{Q}}^{(t)} = \mathbf{Z}^{(t)} - \mathbf{U}^{(t)}$ . The subproblem (27a) can be viewed as a proximal mapping from  $\bar{\mathbf{Q}}^{(t)}$ , which, in contrast, has no closed-form solution. Hence, in Section IV-A, we develop an efficient iterative algorithm for solving subproblem (27a) based on the successive convex approximation (SCA) framework with separable quadratic approximation.

The main steps of the ADMM algorithm for problem (17) are outlined in Algorithm 1. The convergence of ADMM is established under the following conditions [27, Sec. 3.2]:

- 1) the epigraphs of  $f$  and  $g$  in (24) are both closed nonempty sets;
- 2) the unaugmented Lagrangian  $L_0$  has a saddle point, i.e., the strong duality holds.

The above conditions can be readily verified for the considered convex problem (24). Strong duality holds for problem (24) as Slater's condition is satisfied [29, Sec. 5.2.3 and Sec. 5.4.2].

#### A. Successive Convex Approximation for the $\mathbf{Q}$ -update

Since the subproblem for the  $\mathbf{Q}$ -update (27a) is convex, a global optimum can be efficiently obtained by using the SCA framework [30] with separable quadratic approximation. For simplicity, the ADMM iteration index  $t$  in  $\bar{\mathbf{Q}}^{(t)}$  is omitted and the objective function in (27a) is denoted by

$$h(\mathbf{Q}) = f(\mathbf{Q}) + \frac{\rho}{2} \|\mathbf{Q} - \bar{\mathbf{Q}}\|_F^2, \quad (28)$$

as we discuss only the  $\mathbf{Q}$ -update subproblem in a single ADMM iteration. In each iteration, we first construct a separable quadratic approximation for  $h$  by exploiting the shift-invariance structure of  $\mathbf{Q}$  specified by the constraints in (14). To obtain an approximate problem that can be decomposed and solved in parallel, we minimize the quadratic approximate function in a relaxed domain of problem (27a) with the positive definiteness constraint discarded. The solution of the quadratic approximate problem indicates a descent direction of the original function  $h$ . Then, variable  $\mathbf{Q}$  is updated in this descent direction with a suitable step size that ensures sufficient decrease of  $h$  and positive definiteness of  $\mathbf{Q} + \lambda \mathbf{I}_M$  for the intermediate iterates. An Armijo-rule-based backtracking line search is employed to efficiently find the step size.

In the case where  $\hat{\mathbf{R}} \succ 0$ , the term  $\operatorname{tr}((\mathbf{Q} + \lambda \mathbf{I}_M)^{-1} \hat{\mathbf{R}})$  in  $f$  plays the role of a barrier for the set  $\{\mathbf{Q} \in \mathbb{S}^M \mid \mathbf{Q} + \lambda \mathbf{I}_M \succ 0\}$ , i.e., both its function value and gradient tend to  $+\infty$  when the variable  $\mathbf{Q}$  approaches the boundary of the set from the interior. In this case, the exclusion of the positive definiteness constraint in (27a) from the approximate problem does not impact the convergence of the proposed algorithm. In particular, the proposed algorithm is ensured to converge to a global optimum of the convex problem (27a) as it satisfies the regularity conditions of the SCA framework in [30]. In contrast, the above convergence guarantee does not hold in the undersampled case, i.e.,  $N \leq M$ , where  $\hat{\mathbf{R}}$  is always rank deficient. Hence, as mentioned at the beginning of Section IV, in the undersampled case, a small positive diagonal loading onto the sample covariance matrix is required before solving the gridless SPARROW problem (17). Moreover, the proposed algorithm can also be viewed as a variant of diagonal approximation to Newton's method [31], which is shown to have an asymptotically quadratic convergence rate.

1) *Separable Quadratic Approximation:* Using the expression in (21), we design a convex quadratic approximation for the  $\mathbf{Q}$ -update subproblem (27a) that is separable in the independent variables  $\mathbf{q}$ . To this end, we first present the expressions for the gradient and quadratic Taylor expansion of  $f$ . When only the Hermitian structure of  $\mathbf{Q}$ , and not the shift-invariance structural constraints, is considered, the gradient of  $f$  in (24) with respect to  $\mathbf{Q}$  is given by

$$\nabla_{\mathbf{Q}} f(\mathbf{Q}) = -M(\mathbf{Q} + \lambda \mathbf{I}_M)^{-1} \hat{\mathbf{R}}(\mathbf{Q} + \lambda \mathbf{I}_M)^{-1} + \mathbf{I}_M, \quad (29)$$

and the gradient of  $h$  with respect to  $\mathbf{Q}$  is

$$\nabla_{\mathbf{Q}} h(\mathbf{Q}) = \nabla_{\mathbf{Q}} f(\mathbf{Q}) + \rho(\mathbf{Q} - \bar{\mathbf{Q}}). \quad (30)$$

Let  $\mathbf{Q}^{(l)}$  be the approximate solution for problem (27a) in the  $l$ th iteration and  $\mathbf{q}^{(l)}$  be the corresponding values for the independent variables  $\mathbf{q}$ . The quadratic Taylor expansion of  $f$  around  $\mathbf{Q}^{(l)}$  can then be expressed as

$$f(\mathbf{Q}) \approx f(\mathbf{Q}^{(l)}) + \operatorname{tr}(\nabla_{\mathbf{Q}} f(\mathbf{Q}^{(l)}) \mathbf{\Delta}) + M \operatorname{tr}(\mathbf{V} \mathbf{\Delta} \tilde{\mathbf{R}} \mathbf{\Delta}), \quad (31)$$

where  $\mathbf{\Delta} = \mathbf{Q} - \mathbf{Q}^{(l)}$ ,  $\mathbf{V} = (\mathbf{Q}^{(l)} + \lambda \mathbf{I}_M)^{-1}$ , and  $\tilde{\mathbf{R}} = \mathbf{V} \hat{\mathbf{R}} \mathbf{V}$ . The details of the computation of the gradient and quadratic Taylor expansion of  $f$  are provided in Appendix A.

Departing from Newton's method, which iteratively approximates the original objective function  $h$  directly by its quadratic Taylor expansion, to construct an approximate problem that can be decomposed and solved in parallel, we adopt

the following separable quadratic approximation:

$$\begin{aligned} \tilde{h}^{(l)}(\mathbf{q}) &= h(\mathbf{q}^{(l)}) + \sum_{i=1}^I \Re(\nabla_{q_i}^* h(\mathbf{q}^{(l)})(q_i - q_i^{(l)})) \\ &\quad + \sum_{i=1}^I \frac{1}{2} \nabla_{q_i}^2 h(\mathbf{q}^{(l)}) |q_i - q_i^{(l)}|^2, \end{aligned} \quad (32)$$

which preserves only the diagonal entries of the Hessian of  $h$  with respect to the independent variables  $\mathbf{q}$  at the current point  $\mathbf{q}^{(l)}$ . From the results in (30) and (31), the partial gradient and Hessian of  $h$  with respect to an independent variable  $q_i$  can be calculated by the chain rule of differentiation as

$$\nabla_{q_i} h(\mathbf{q}^{(l)}) = 2 \operatorname{tr}(\mathbf{\Omega}_i^T \cdot \nabla_{\mathbf{Q}} h(\mathbf{Q}^{(l)})) \quad \text{and} \quad (33a)$$

$$\nabla_{q_i}^2 h(\mathbf{q}^{(l)}) = 2 \left( M \operatorname{tr}(\tilde{\mathbf{R}}(\mathbf{\Omega}_i^T \mathbf{V} \mathbf{\Omega}_i + \mathbf{\Omega}_i \mathbf{V} \mathbf{\Omega}_i^T)) + \rho \|\mathbf{\Omega}_i\|_F^2 \right) \quad (33b)$$

for  $i = 2, \dots, I$ . Recall that the matrix  $\mathbf{\Omega}_i$  defined in (20) indicates the entries of  $\mathbf{Q}$  occupied by the independent variable  $q_i$ . For the real-valued variable  $q_1$  on the diagonal of the matrix  $\mathbf{Q}$ , the factor of two in (33b) and (33a) needs to be removed.

Then the following separable approximate problem is constructed at the  $l$ th iteration:

$$\tilde{q}_1^{(l)} = \operatorname{argmin}_{q_1 \in \mathbb{C}^I} \tilde{h}^{(l)}(\mathbf{q}) \quad \text{s.t.} \quad q_1 \geq -\lambda, \quad (34)$$

where, as aforementioned, the positive definiteness constraint in (27a) is relaxed to a trivial separable bounding constraint. Problem (34) can be decomposed into  $I$  independent subproblems. Each subproblem depends exclusively on a single variable in  $\mathbf{q}$  and, hence, can be solved in parallel. Specifically, each subproblem is a univariate convex quadratic program, which admits the following closed-form solution:

$$\tilde{q}_i^{(l)} = q_i^{(l)} - \frac{\nabla_{q_i} h(\mathbf{q}^{(l)})}{\nabla_{q_i}^2 h(\mathbf{q}^{(l)})} \quad \text{for } i = 2, \dots, I. \quad (35)$$

Recall that all diagonal elements of the matrix  $\mathbf{Q}$  are identical and real-valued, which are represented by the independent variable  $q_1$ . With the bounding constraint in (34), the solution of the subproblem involving  $q_1$  is given by

$$\tilde{q}_1^{(l)} = \max \left\{ -\lambda, q_1^{(l)} - \frac{\nabla_{q_1} h(\mathbf{q}^{(l)})}{\nabla_{q_1}^2 h(\mathbf{q}^{(l)})} \right\}. \quad (36)$$

The matrix  $\tilde{\mathbf{Q}}^{(l)}$  corresponding to  $\tilde{q}_1^{(l)}$  is then computed according to (21), which, unfortunately, may not satisfy the positive definiteness constraint in (27a). Therefore, the following line search is performed to obtain the next iterate in the feasible set of problem (27a) based on the solution  $\tilde{\mathbf{Q}}^{(l)}$ .

Define  $\mathbf{\Delta}^{(l)} = \tilde{\mathbf{Q}}^{(l)} - \mathbf{Q}^{(l)}$ . The difference  $\mathbf{\Delta}^{(l)}$  is a descent direction of the original objective function  $h$  due to the consistency of the gradient at the current point  $\mathbf{Q}^{(l)}$  between  $h$  and the separable quadratic approximation  $\tilde{h}^{(l)}$ . Thus, the following update rule can be applied:

$$\mathbf{Q}^{(l+1)} = \mathbf{Q}^{(l)} + \alpha^{(l)} \mathbf{\Delta}^{(l)} \quad (37)$$

with a suitable step size  $\alpha^{(l)} \in (0, 1]$  that ensures a sufficient decrease of the original objective function  $h$  and the positive definiteness of  $\mathbf{Q}^{(l+1)} + \lambda \mathbf{I}_M$ . Moreover, when  $\tilde{\mathbf{Q}}^{(l)} = \mathbf{Q}^{(l)}$ , a stationary point of  $\tilde{h}^{(l)}$  is achieved, which is also a stationary point and global optimum of the original function  $h$  due to the gradient consistency [30, Thm. 1].

2) *Step Size Computation for the  $\mathbf{Q}$ -update subproblem:*

The Armijo-rule-based backtracking line search can be employed to find a suitable step size for the update in (37) at a

low computational cost. In the Armijo rule, we successively try step sizes  $\alpha \in \{\beta^0, \beta^1, \dots\}$ , i.e., a geometric sequence with a constant decrease rate  $0 < \beta < 1$ , until we find the smallest  $k \in \mathbb{N}$  with  $\alpha = \beta^k$  such that  $\mathbf{Q}^{(l)} + \alpha \mathbf{\Delta}^{(l)}$  satisfies the positive definiteness constraint in (27a), i.e.,  $\mathbf{Q}^{(l)} + \alpha \mathbf{\Delta}^{(l)} + \lambda \mathbf{I}_M \succ 0$ , and the following sufficient decrease condition:

$$h(\mathbf{Q}^{(l)} + \alpha \mathbf{\Delta}^{(l)}) \leq h(\mathbf{Q}^{(l)}) + \alpha \sigma \operatorname{tr}(\nabla h(\mathbf{Q}^{(l)})^H \mathbf{\Delta}^{(l)}), \quad (38)$$

where  $0 < \sigma < 1$ . The positive definiteness can be verified while we compute the Cholesky decomposition that is required for the matrix inversion in the objective function evaluation. The computational cost in the step size computation is dominated by the Cholesky decomposition (costs  $n^3/3$  flops). Additionally, we remark that, if we adopt the standard convention in convex analysis that  $h(\mathbf{Q})$  is defined as  $+\infty$  for all  $\mathbf{Q}$  not in the feasible set of problem (27a), which is known as extended-value extension [29], then condition (38) implicitly enforces the positive definiteness of  $\mathbf{Q}^{(l)} + \alpha \mathbf{\Delta}^{(l)} + \lambda \mathbf{I}_M$ .

3) *Stopping Criterion for the  $\mathbf{Q}$ -update subproblem:* Provided that  $\tilde{\mathbf{R}} \succ 0$ , a feasible point  $\mathbf{q}$  is a global optimal solution of the convex problem (27a) if and only if it satisfies the stationarity condition  $\nabla_{\mathbf{q}} h(\mathbf{q}) = \mathbf{0}$ . Thus, Algorithm 2 for solving the  $\mathbf{Q}$ -update subproblem (27a) in an ADMM iteration is terminated when the gradient at the  $l$ th iteration is sufficiently small, i.e., with a given tolerance  $\eta > 0$ ,

$$\|\nabla_{\mathbf{q}} h(\mathbf{q}^{(l)})\|_2 \leq \sqrt{I} \eta. \quad (39)$$

Finally, the proposed SCA-based algorithm for the  $\mathbf{Q}$ -update subproblem (27a) is outlined in Algorithm 2. As for the initialization, the variable  $\mathbf{Q}$  is simply initialized to be the current value  $\mathbf{Q}^{(t)}$  in the ADMM iteration.

## B. Initialization

Provided that the sample covariance matrix  $\hat{\mathbf{R}}$  is positive definite, the objective function  $f(\mathbf{Q}) = M \operatorname{tr}((\mathbf{Q} + \lambda \mathbf{I}_M)^{-1} \hat{\mathbf{R}}) + \operatorname{tr}(\mathbf{Q})$  in (17) is convex in the set  $\{\mathbf{Q} \in \mathbb{S}^M \mid \mathbf{Q} + \lambda \mathbf{I}_M \succ 0\}$  and, hence, has a unique minimum point, which can be obtained by solving the stationarity condition

$$\nabla_{\mathbf{Q}} f(\mathbf{Q}) = \mathbf{0} \quad \text{for } \mathbf{Q} + \lambda \mathbf{I}_M \succ 0 \quad (40)$$

with  $\nabla_{\mathbf{Q}} f$  given in (29). That is, the relaxed problem

$$\hat{\mathbf{Q}}_1 = \operatorname{argmin}_{\mathbf{Q} \in \mathbb{S}^M} f(\mathbf{Q}) \quad \text{s.t.} \quad \mathbf{Q} + \lambda \mathbf{I}_M \succ 0 \quad (41)$$

admits the closed-form solution

$$\hat{\mathbf{Q}}_1 = \sqrt{M \hat{\mathbf{R}}^{\frac{1}{2}}} - \lambda \mathbf{I}_M, \quad (42)$$

which is obtained from the stationarity condition in (40).

Due to the noise in the measurements,  $\hat{\mathbf{Q}}_1$  is not guaranteed to be PSD and satisfy the shift-invariance constraints. Therefore, we then solve the following relaxation to (24):

$$\hat{\mathbf{Q}}_2 = \operatorname{argmin}_{\mathbf{Q} \in \mathcal{T}^M} f(\mathbf{Q}) \quad \text{s.t.} \quad \mathbf{Q} + \lambda \mathbf{I}_M \succ 0, \quad (43)$$

where the auxiliary variable  $\mathbf{Z}$  used to enforce the positive semidefiniteness of  $\mathbf{Q}$  is discarded. The relaxed problem (43) can be viewed as an instance of the  $\mathbf{Q}$ -update subproblem (27a) with the penalty parameter  $\rho = 0$ . Hence, problem (43) can be solved by Algorithm 2 with an initialization  $\mathbf{Q}^{(0)} = \mathcal{P}_{\mathcal{T}^M}(\hat{\mathbf{Q}}_1) + \iota \mathbf{I}_M$ , where  $\iota \geq 0$  is chosen to ensure the positive definiteness of  $\mathbf{Q}^{(0)} + \lambda \mathbf{I}_M$ . The projection onto set  $\mathcal{T}^M$  is easily implemented by averaging the entries corresponding to the same independent variable.

If the solution  $\widehat{\mathbf{Q}}_2$  of (43) is PSD, then it is also the optimal solution of problem (24) and there is no need to perform the ADMM iterations in (27). This also implies that the dual optimal solution  $\widehat{\mathbf{U}}$  for (24) is all zero. Otherwise,  $\widehat{\mathbf{Q}}_2$  is chosen to be the initial value  $\mathbf{Q}^{(0)}$  for the ADMM iterations. Variables  $\mathbf{Z}$  and  $\mathbf{U}$  are then initialized to be  $\mathbf{Z}^{(0)} = \mathcal{P}_{\mathbb{S}_+^M}(\mathbf{Q}^{(0)})$  and  $\mathbf{U}^{(0)} = \mathbf{Q}^{(0)} - \mathbf{Z}^{(0)}$ , respectively.

### C. Stopping Criterion for the ADMM

In the ADMM Algorithm 1, the primal and dual residuals at the  $t$ th iteration are defined as

$$\mathbf{\Gamma}_{\text{pri}}^{(t)} = \mathbf{Q}^{(t)} - \mathbf{Z}^{(t)} \quad \text{and} \quad \mathbf{\Gamma}_{\text{dual}}^{(t)} = -\rho(\mathbf{Z}^{(t)} - \mathbf{Z}^{(t-1)}), \quad (44)$$

respectively. A global optimum of problem (24) is achieved if and only if both  $\mathbf{\Gamma}_{\text{pri}}^{(t)}$  and  $\mathbf{\Gamma}_{\text{dual}}^{(t)}$  vanish. Therefore, as suggested in [27], a reasonable stopping criterion for Algorithm 1 is that the primal and dual residuals must be small, i.e.,

$$\|\mathbf{\Gamma}_{\text{pri}}^{(t)}\|_{\text{F}} \leq \varepsilon^{\text{pri}} \quad \text{and} \quad \|\mathbf{\Gamma}_{\text{dual}}^{(t)}\|_{\text{F}} \leq \varepsilon^{\text{dual}}, \quad (45)$$

where  $\varepsilon^{\text{pri}} > 0$  and  $\varepsilon^{\text{dual}} > 0$  are the tolerances for the primal and dual residuals, respectively. Those tolerances can be chosen by using an absolute and relative criterion, such as

$$\begin{aligned} \varepsilon^{\text{pri}} &= M\varepsilon^{\text{abs}} + \varepsilon^{\text{rel}} \cdot \max(\|\mathbf{Q}^{(t)}\|_{\text{F}}, \|\mathbf{Z}^{(t)}\|_{\text{F}}), \\ \varepsilon^{\text{dual}} &= M\varepsilon^{\text{abs}} + \varepsilon^{\text{rel}} \cdot \|\rho\mathbf{U}^{(t)}\|_{\text{F}}, \end{aligned} \quad (46)$$

where  $\varepsilon^{\text{abs}} > 0$  is an absolute tolerance and  $\varepsilon^{\text{rel}} > 0$  a relative tolerance, and the variable size is also taken into account.

### D. Choice of Penalty Parameter $\rho$

The choice of the penalty parameter  $\rho$  in ADMM in practice has a strong impact on the convergence rate and is a demanding task. As an extension to the classical ADMM algorithm, different penalty parameters  $\rho^{(t)}$  can be adaptively chosen for each iteration so that the performance is less dependent on the initial choice of the penalty parameter. The following scheme is recommended in [27, Sec. 3.4.1]: given  $\rho^{(0)}$ ,

$$\rho^{(t+1)} = \begin{cases} \tau^{\text{incr}} \rho^{(t)} & \text{if } \|\mathbf{\Gamma}_{\text{pri}}^{(t)}\|_{\text{F}} > \kappa \|\mathbf{\Gamma}_{\text{dual}}^{(t)}\|_{\text{F}} \text{ and } t \leq t_{\text{max}}, \\ \rho^{(t)} / \tau^{\text{decr}} & \text{if } \|\mathbf{\Gamma}_{\text{dual}}^{(t)}\|_{\text{F}} > \kappa \|\mathbf{\Gamma}_{\text{pri}}^{(t)}\|_{\text{F}} \text{ and } t \leq t_{\text{max}}, \\ \rho^{(t)} & \text{otherwise,} \end{cases} \quad (47)$$

where  $\kappa > 1$ ,  $\tau^{\text{incr}} > 1$ ,  $\tau^{\text{decr}} > 1$ , and  $t_{\text{max}} > 0$  are tuning parameters. The penalty parameter  $\rho$  is fixed after  $t_{\text{max}}$  iterations in order to ensure the convergence [32], [33]. Note that, as  $\mathbf{U}$  represents the dual variable scaled by  $1/\rho$ , it must be rescaled when  $\rho$  is updated.

## V. SUCCESSIVE CONVEX APPROXIMATION FOR SHIFT-INVARIANT SPARROW

As discussed in Section IV, the convergence of the ADMM Algorithm 1 requires the positive semidefiniteness of the sample covariance matrix  $\widehat{\mathbf{R}}$ . Hence, in the undersampled case, where  $\widehat{\mathbf{R}}$  is always rank deficient, a small positive diagonal loading onto  $\widehat{\mathbf{R}}$  is performed, which, however, may result in a degradation of the estimation quality. On the other hand, the SDP approach based on the reformulation in (19) or (18) relies on an efficient general-purpose SDP solver, which often has high hardware requirements and implementation costs. Thus,

---

### Algorithm 3: SCA Algorithm for SI-SPARROW.

---

**Input:** Sample covariance matrix  $\widehat{\mathbf{R}}$ , indicator matrices  $\{\Omega_i\}_{i=1}^I$ , regularization parameter  $\lambda > 0$ , tolerances  $\varepsilon^{\text{abs}}, \varepsilon^{\text{rel}} > 0$

- 1 Initialize  $\mathbf{Q}^{(0)}, t \leftarrow 0$ ;
- 2 **while not converged do**
- 3     Compute  $\widetilde{\mathbf{Q}}^{(t)}$  by solving the approximate problem (50) using ADMM algorithm;
- 4     Compute step size  $\alpha^{(t)}$  by Armijo rule;
- 5      $\mathbf{Q}^{(t+1)} \leftarrow \mathbf{Q}^{(t)} + \alpha^{(t)}(\widetilde{\mathbf{Q}}^{(t)} - \mathbf{Q}^{(t)})$ ;
- 6      $t \leftarrow t + 1$ ;
- 7 **return**  $\mathbf{Q}^{(t)}$

---

in this section, by switching the inner and outer iterations in Algorithm 1, we develop an alternative algorithm for the SI-SPARROW problem (17) with guaranteed convergence that does not require the positive semidefiniteness of the sample covariance matrix and can be implemented on relatively low-cost hardware. In particular, we apply the SCA framework directly on the SI-SPARROW problem (17), where a descent direction of the function  $f$  in (17) in the intersection  $\mathbb{S}_+^M \cap \mathcal{T}^M$  is obtained by solving a quadratic approximate problem and then the backtracking line search is employed to update the variable  $\mathbf{Q}$  along the descent direction with a suitable step size that ensures sufficient decrease of  $f$ . Nevertheless, unlike Algorithm 2 for the  $\mathbf{Q}$ -update subproblem in (27a), the quadratic approximation for the original problem (17) cannot be solved in closed form since the variable  $\mathbf{Q}$  is required to be in both the PSD cone  $\mathbb{S}_+^M$  and the shift-invariant subspace  $\mathcal{T}^M$ . Hence, the ADMM framework is used to iteratively solve the quadratic approximation in an inner loop by separating the PSD constraint from the shift-invariance constraints.

Similar to the approximation in (32), to obtain an approximate problem that can be solved in parallel at a low computational cost, we construct the separable quadratic approximation

$$\begin{aligned} \widetilde{f}^{(t)}(\mathbf{q}) &= f(\mathbf{q}^{(t)}) + \sum_{i=1}^I \Re(\nabla_{q_i}^* f(\mathbf{q}^{(t)})(q_i - q_i^{(t)})) \\ &\quad + \sum_{i=1}^I \frac{1}{2} \nabla_{q_i}^2 f(\mathbf{q}^{(t)}) |q_i - q_i^{(t)}|^2, \end{aligned} \quad (48)$$

which preserves only the diagonal entries of the Hessian of the original function  $f$  in (17) with respect to the independent variables  $\mathbf{q}$  at the current point  $\mathbf{q}^{(t)}$ . In (48), the partial Hessian and gradient of  $f$  with respect to an independent variable  $q_i$  can likewise be calculated by the chain rule of differentiation from the results in (29) and (31). They are expressed as

$$\nabla_{q_i}^2 f(\mathbf{q}^{(t)}) = 2M \operatorname{tr}(\widetilde{\mathbf{R}}(\Omega_i^{\text{T}} \mathbf{V} \Omega_i + \Omega_i \mathbf{V} \Omega_i^{\text{T}})), \quad (49a)$$

$$\nabla_{q_i} f(\mathbf{q}^{(t)}) = 2 \operatorname{tr}(\Omega_i^{\text{T}} \cdot \nabla_{\mathbf{Q}} f(\mathbf{Q}^{(t)})), \quad (49b)$$

with  $\mathbf{V} = (\mathbf{Q}^{(t)} + \lambda \mathbf{I}_M)^{-1}$  and  $\widetilde{\mathbf{R}} = \mathbf{V} \widehat{\mathbf{R}} \mathbf{V}$  for  $i = 1, \dots, I$ . For the real-valued variable  $q_1$  at the main diagonal of matrix  $\mathbf{Q}$ , the factor of two in (49a) and (49b) needs to be removed. Then the quadratic approximation for the original SI-SPARROW problem (17) at the  $t$ th iteration reads as

$$\widetilde{\mathbf{Q}}^{(t)} = \operatorname{argmin}_{\mathbf{Q} \in \mathbb{S}_+^M \cap \mathcal{T}^M} \widetilde{f}^{(t)}(\mathbf{Q}). \quad (50)$$

Although the quadratic approximate function  $\widetilde{f}^{(t)}$  is separa-



ble in the independent variables  $\mathbf{q}$ , problem (50), unfortunately, cannot be solved in closed form due to the PSD constraint. Due to the convexity of the original function  $f$ , the approximate function  $\tilde{f}^{(t)}$  is a convex quadratic function. Thus, problem (50) can be viewed as a projection onto the intersection of two convex sets, i.e., the PSD cone  $\mathbb{S}_+^M$  and the shift-invariant subspace  $\mathcal{T}^M$ , which can be conventionally solved by the alternating projection [34] that finds the projection onto the intersection by alternately projecting onto each of the two sets. On the other hand, the ADMM framework, when applied to the projection problem in (50), reduces to the Dykstra's alternating projection [27], [35], which is shown to be far more efficient than the classical alternating projection that does not use a dual variable [36]. Hence, we employ the ADMM algorithm to solve the quadratic approximate problem (50), which, similar to (27), consists of the following steps in the  $l$ th inner-iteration:

$$\mathbf{Q}^{(l+1)} = \underset{\mathbf{Q} \in \mathcal{T}^M}{\operatorname{argmin}} \tilde{f}^{(t)}(\mathbf{Q}) + \frac{\rho}{2} \|\mathbf{Q} - \mathbf{Z}^{(l)} + \mathbf{U}^{(l)}\|_F^2, \quad (51a)$$

$$\mathbf{Z}^{(l+1)} = \mathcal{P}_{\mathbb{S}_+^M}(\mathbf{Q}^{(l+1)} + \mathbf{U}^{(l)}), \quad (51b)$$

$$\mathbf{U}^{(l+1)} = \mathbf{U}^{(l)} + \mathbf{Q}^{(l+1)} - \mathbf{Z}^{(l+1)}. \quad (51c)$$

In contrast to (27), the  $\mathbf{Q}$ -update subproblem in (51a) can be solved in closed-form since problem (51a) is an unconstrained quadratic program in the independent variables  $\mathbf{q}$ . Moreover, as the approximate function  $\tilde{f}^{(t)}$  is designed to be separable in the independent variables  $\mathbf{q}$ , problem (51a) can be decomposed into  $I$  quadratic subproblems, each of which exclusively depends on a single independent variable  $q_i$ . Hence, the closed-form solution of problem (51a) can be calculated in parallel for each independent variable  $q_i$ .

The convergence of the proposed Algorithm 3 is readily established in the SCA framework [30]. Specifically, due to the consistency of the gradient at the current point  $\mathbf{Q}^{(t)}$  between the original objective function  $f$  and the quadratic approximation  $\tilde{f}^{(t)}$ , when  $\tilde{\mathbf{Q}}^{(t)} = \mathbf{Q}^{(t)}$ , a stationary point of  $\tilde{f}^{(t)}$  is achieved, which is also a stationary point and global optimum of the original function  $f$  in the set  $\mathbb{S}_+^M \cap \mathcal{T}^M$ . Otherwise, define  $\Delta^{(t)} = \tilde{\mathbf{Q}}^{(t)} - \mathbf{Q}^{(t)}$ . The difference  $\Delta^{(t)}$  is a descent direction of  $f$  in the set  $\mathbb{S}_+^M \cap \mathcal{T}^M$ . Thus, the matrix  $\mathbf{Q}$  can be updated according to the rule

$$\mathbf{Q}^{(t+1)} = \mathbf{Q}^{(t)} + \alpha^{(t)} \Delta^{(t)} \quad (52)$$

with a suitable step size  $\alpha^{(t)} \in [0, 1]$  that ensures a sufficient decrease of the original objective function  $f$ . The step size  $\alpha^{(t)}$  can be obtained by an Armijo-rule-based back-tracking line search similar to that described in Section IV-A. Nevertheless, since the approximate solution  $\tilde{\mathbf{Q}}^{(t)}$  is found in the original feasible set  $\mathbb{S}_+^M \cap \mathcal{T}^M$ , the feasibility of the matrix  $\mathbf{Q}^{(t+1)}$  is guaranteed by the convexity of the set  $\mathbb{S}_+^M \cap \mathcal{T}^M$  and does not require additional verification.

Neither the subgradient of the extended-value extension of the original function  $f$  nor that of the quadratic approximation  $\tilde{f}$  can be easily obtained at the boundary of the original feasible set  $\mathbb{S}_+^M \cap \mathcal{T}^M$ . Therefore, in contrast to the evaluation of stationarity in Section IV, we simply terminate Algorithm 3 when the change of  $\mathbf{Q}$  is sufficiently small, i.e., with an absolute tolerance  $\varepsilon^{\text{abs}} > 0$  and a relative tolerance  $\varepsilon^{\text{rel}} > 0$ ,

$$\|\mathbf{Q}^{(t)} - \mathbf{Q}^{(t-1)}\|_F \leq M\varepsilon^{\text{abs}} + \varepsilon^{\text{rel}}\|\mathbf{Q}^{(t-1)}\|_F \quad (53)$$

The proposed algorithm for problem (17) in the SCA framework is outlined in Algorithm 3. The matrix  $\mathbf{Q}$  is initialized as  $\mathbf{Q}^{(0)} = \mathcal{P}_{\mathcal{T}^M}(\hat{\mathbf{Q}}_1) + \iota \mathbf{I}_M$ , where  $\hat{\mathbf{Q}}_1$  given in (42) corresponds to the optimal solution of the relaxed problem (41) if the sample covariance matrix  $\hat{\mathbf{R}}$  is positive definite, and  $\iota \geq 0$  is chosen to ensure the positive semidefiniteness of  $\mathbf{Q}^{(0)}$ .

## VI. GENERALIZATION TO UNOBSERVABLE SENSORS

In this section, we briefly introduce a generalization of the SI-SPARROW method to the case where part of the sensors are unobservable due to failure.

We consider the same PCRA of  $M$  sensors with the shift-invariance properties in (6) as introduced in Section II. In this section, we additionally assume that part of the sensors are unobservable due to failure. In some other scenarios, the unobservable sensors may be virtual sensors introduced for exploiting additional shift-invariance properties. In particular, let  $M' \leq M$  be the number of observable sensors and  $\mathcal{M}' = \{i_1, \dots, i_{M'}\}$  denotes the set of the indices of the observable sensors. Define the selection matrix

$$\mathbf{J}_{\mathcal{M}'} = [e_{M, i_1} \quad \cdots \quad e_{M, i_{M'}}] \in \mathbb{R}^{M \times M'}. \quad (54)$$

Then the matrix

$$\mathbf{Y}' = \mathbf{J}_{\mathcal{M}'}^T \mathbf{Y} \in \mathbb{C}^{M' \times N} \quad (55)$$

contains the responses of the  $M'$  observable sensors in  $N$  time-slots. To address the issue with unobservable sensors, a simple modification of the SI-SPARROW method introduced in Section III is to reconstruct or discard the part of the shift-invariance constraints that involve the responses of the unobservable sensors. This, however, leads to a significant degradation of the estimation quality. Therefore, we introduce a generalization of the SI-SPARROW method that, while using only the measurements from the observable sensors, i.e., the matrix  $\mathbf{Y}'$ , for the data fidelity, preserves all the shift-invariance properties stated in (6) in the complete array.

When only the measurements in the matrix  $\mathbf{Y}'$  are taken into consideration for the data fidelity, the DOA estimation problem based on the sparse model in (8) is then formulated as the following convex mixed-norm minimization problem:

$$\min_{\mathbf{X} \in \mathbb{C}^{K \times N}} \frac{1}{2} \|\mathbf{Y}' - \mathbf{J}_{\mathcal{M}'}^T \mathbf{A} \mathbf{X}\|_F^2 + \lambda \sqrt{N} \|\mathbf{X}\|_{2,1}. \quad (56)$$

Similar to problem (10), problem (56) can be equivalently rewritten as the following compact form:

$$\min_{\mathbf{S} \in \mathbb{D}_+^K} \operatorname{tr}((\mathbf{J}_{\mathcal{M}'}^T \mathbf{A} \mathbf{S} \mathbf{A}^H \mathbf{J}_{\mathcal{M}'} + \lambda \mathbf{I}_{M'})^{-1} \hat{\mathbf{R}}) + \operatorname{tr}(\mathbf{S}) \quad (57)$$

with  $\hat{\mathbf{R}}' = \mathbf{Y}'(\mathbf{Y}')^H/N$ . Then we construct the following gridless relaxation of problem (57) by replacing  $\mathbf{A} \mathbf{S} \mathbf{A}^H$  by a matrix  $\mathbf{Q}$  that preserves the shift-invariance properties in (14):

$$\min_{\mathbf{Q} \in \mathbb{S}_+^M \cap \mathcal{T}^M} M \operatorname{tr}((\mathbf{J}_{\mathcal{M}'}^T \mathbf{Q} \mathbf{J}_{\mathcal{M}'} + \lambda \mathbf{I}_{M'})^{-1} \hat{\mathbf{R}}) + \operatorname{tr}(\mathbf{Q}). \quad (58)$$

Likewise, problem (58) can be equivalently reformulated as an SDP problem by the reformulation technique in Section III, and then, solved by an interior-point solver. Alternatively, the ADMM Algorithm 1 proposed in Section IV and the SCA Algorithm 3 in Section V for the original SI-SPARROW problem in (17) can be easily adapted for solving problem (58) with unobservable sensors. The details of the solution approaches for problem (58) are omitted due to space limitations.

## VII. SIMULATION RESULTS

In this section, we conduct numerical experiments on synthetic data to evaluate and analyze the performance of the developed SI-SPARROW method for a PCRA. The complexity of the SDP approach, the ADMM algorithm developed in Section IV, and the SCA algorithm in Section V is also evaluated. The SDP reformulation is modeled by CVX [37], [38] and solved by the efficient interior-point solver MOSEK [21]. As described in Section III-D, from the reconstructed matrix  $\hat{\mathbf{Q}}$ , the spatial frequencies can be recovered by the MI-MD-ESPRIT method that is implemented using the simultaneous diagonalization or Schur decomposition [19], [26], given the shift-invariance equations in (6b) and (6d) with the known sensor displacements  $\delta_l^x$  and  $\delta_l^y$  within each subarray. The estimation error of the proposed method is compared to that of the conventional approach where the MI-MD-ESPRIT method is performed on the sample covariance matrix  $\hat{\mathbf{R}}$ . Moreover, since the centro-symmetric arrays are used in the simulations, we also perform the multidimensional Unitary ESPRIT (MD-Unitary-ESPRIT) [17], [20] on the sample covariance matrix  $\hat{\mathbf{R}}$ . The MD-Unitary-ESPRIT method is also implemented using the simultaneous Schur decomposition and employs only a single shift-invariance equation in each dimension.

We remark that the proposed SI-SPARROW formulation in (17) can also be applied to the fully calibrated case as neither the intersubarray displacements  $\Delta_p^x$  and  $\Delta_p^y$  nor the intrasubarray displacements  $\delta_l^x$  and  $\delta_l^y$  are involved in the shift-invariance constraints (14) for the variable  $\mathbf{Q}$ . Hence, as a comparison, we also evaluate the proposed SI-SPARROW method in the fully calibrated case where, from the solution of SI-SPARROW, the frequencies are recovered by the MUSIC method [1] with the knowledge of both the intersubarray and intrasubarray displacements. Similarly, the performance of SI-SPARROW in the fully calibrated case is compared to that of the conventional approach where MUSIC is performed on the sample covariance matrix. In the MUSIC method, the frequencies are recovered by grid search over the 2D MUSIC spectrum. The grid refinement strategy is used to reduce the complexity of the 2D grid search. In particular, since the stochastic Cramér-Rao Bound (CRB) [9], [39] is calculated as a reference for the performance evaluation in both partly and fully calibrated cases, the grid spacing in MUSIC is successively refined around each estimated DOA until the spacing is negligible compared to the fully calibrated CRB. Additionally, the details of the derivation of the stochastic CRB in the partly calibrated case for the estimation of the spatial frequencies according to the signal model in (2) are given in Appendix B.

The results are averaged over  $N_R = 1000$  Monte-Carlo trials. The estimated frequencies  $\hat{\boldsymbol{\mu}}(n) = [\hat{\mu}_1^x(n), \dots, \hat{\mu}_{N_S}^x(n)]^T$  for  $n = 1, \dots, N_R$  are evaluated by the root-mean-square error (RMSE) with respect to the ground-truth  $\boldsymbol{\mu}$  defined as

$$\text{RMSE}(\hat{\boldsymbol{\mu}}) = \sqrt{\frac{1}{N_S N_R} \sum_{n=1}^{N_R} \sum_{i=1}^{N_S} |\hat{\mu}_i^x(n) - \mu_i^x|_{\text{wa}}^2 + |\hat{\mu}_i^y(n) - \mu_i^y|_{\text{wa}}^2},$$

where  $\hat{\mu}_i^x(n)$  and  $\hat{\mu}_i^y(n)$  denote the estimates of the frequencies of source  $i$  in x-axis and y-axis, respectively, in the  $n$ th trial,

and  $|\mu_1 - \mu_2|_{\text{wa}} = \min_{k \in \mathbb{Z}} |\mu_1 - \mu_2 + 2k\pi|$  denotes the wrap-around distance between two frequencies  $\mu_1$  and  $\mu_2$ . All the experiments were conducted on a Linux PC with an Intel Core i7-7700 CPU and 32 GB RAM running MATLAB R2023a.

In the simulations, we consider  $N_S = 2$  sources with spatial frequencies  $\boldsymbol{\mu}^x = [0.5, 0.8]^T$  and  $\boldsymbol{\mu}^y = [1.5, 1.2]^T$  that follow a zero-mean complex normal distribution with unit variance and the correlation coefficient is denoted by  $\varphi$ . Furthermore, the simulation scenario includes a PCRA consisting of  $2 \times 2$  subarrays. Each subarray is a uniform rectangular array with half-wavelength sensor spacing and, if not further specified, each subarray contains  $L_x = 4$  and  $L_y = 2$  sensors in the two dimensions, respectively. The intersubarray displacements measured in half signal wavelength in the two dimensions are set to be  $\Delta_2^x = L_x + 49$  and  $\Delta_2^y = L_y + 49$ . Only the sensor spacing within each subarray is known for the frequency recovery. The SNR is calculated as  $1/\sigma_n^2$ .

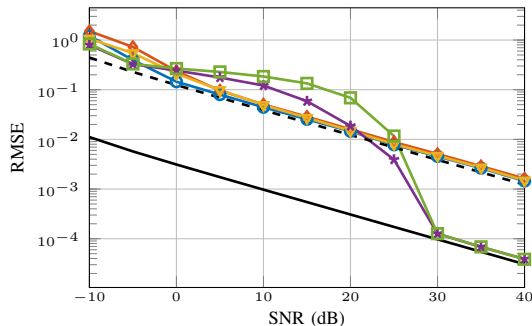
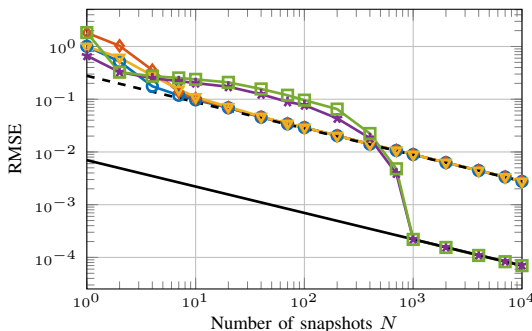
Some algorithmic parameters are set as follows. Although the normalized steering vector model is used in [15], the tuning rule for the regularization parameter proposed in [15] can be readily adapted to the unnormalized steering vector model considered in this paper, which is  $\lambda = \sqrt{M} \sigma_n (\sqrt{M/N} + 1)$ . However, in our simulations, to reduce the performance degradation and the asymptotic bias that results from the  $\ell_{2,1}$ -regularization, we reduce the regularization parameter  $\lambda$  to

$$\lambda = \sigma_n (\sqrt{M/N} + 1). \quad (59)$$

In the ADMM algorithm, the adaptive varying scheme in (47) for the penalty parameter  $\rho$  is used as it typically improves the convergence in practice. The tuning parameters in (47) are chosen as  $\kappa = 10$ ,  $\tau^{\text{incr}} = \tau^{\text{decr}} = 2$ ,  $\tau_{\text{max}} = 50$ , and  $\rho^0 = 1$ . Suitable termination tolerances are selected for different algorithms so that they achieve similar precisions on the estimation quality. Specifically, both the absolute and the relative tolerance in (46) for the termination of the ADMM Algorithm 1 are set to be  $10^{-4}$ , whereas, for the SCA Algorithm 3, the absolute and relative tolerances are chosen to be  $10^{-5}$ .

### A. Uncorrelated Source Signals

We first compare the error performance of the methods in the case with uncorrelated source signals, i.e., with the correlation coefficient  $\varphi = 0$ . The estimation errors of the evaluated methods for various choices of SNR and the number of snapshots are reported in Fig. 3. In the partly calibrated case, as observed in both Fig. 3(a) and 3(b), when performed on the sample covariance matrix  $\hat{\mathbf{R}}$ , both MI-MD-ESPRIT and MD-Unitary-ESPRIT have the same threshold, which is larger than that of SI-SPARROW. However, compared to MI-MD-ESPRIT, MD-Unitary-ESPRIT shows superior estimation quality in the threshold region. Moreover, all three evaluated partly calibrated methods exhibit almost identical estimation errors in the asymptotic region. Likewise, in the fully calibrated case, in comparison to the MUSIC method performed on the sample covariance matrix, the MUSIC method performed on the solution of SI-SPARROW shows similar threshold and asymptotic performance but has a slightly improved estimation quality before the threshold. In addition, it is somewhat surprising that, although more information is

(a) RMSE vs. SNR for  $N = 5$  snapshots

(b) RMSE vs. the number of snapshots for SNR = 0 dB

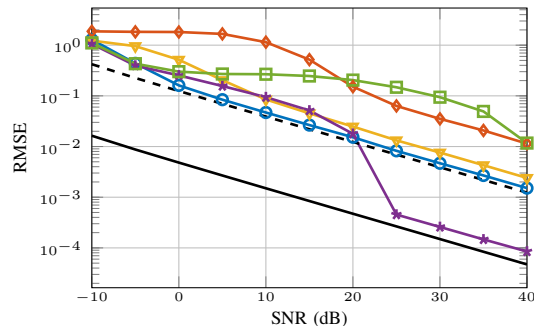
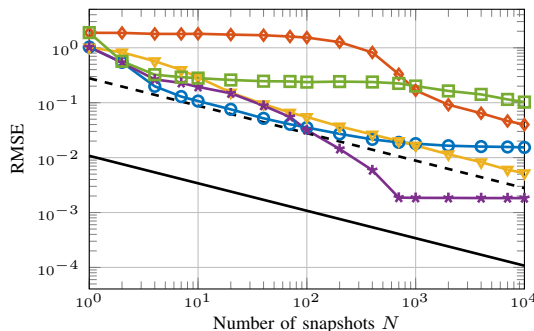
Fig. 3. Error performance for  $N_S = 2$  uncorrelated sources with spatial frequencies  $\boldsymbol{\mu}^x = [0.5, 0.8]^T$  and  $\boldsymbol{\mu}^y = [1.5, 1.2]^T$ .

used in the considered fully calibrated methods, they provide an error performance inferior to that of the partly calibrated methods in the region where their RMSE has not achieved the fully calibrated CRB.

### B. Correlated Source Signals

We then evaluate the error performance of the methods in the case with correlated source signals. In particular, the correlation coefficient between the two sources is chosen to be  $\varphi = 0.99$ . The estimation errors of the evaluated methods for various choices of SNR and the number of snapshots are likewise presented in Fig. 4.

We first compare the performance of the partly calibrated methods. Similar to the conclusions in [3], Fig. 4 demonstrates that, while standard ESPRIT, which is performed in MI-MD-ESPRIT, admits a significant degradation of the estimation quality in the case with correlated sources, the incorporation of forward-backward averaging in Unitary-ESPRIT typically leads to an enhanced error performance compared to standard ESPRIT. As discussed at the beginning of this section, the MD-Unitary-ESPRIT method can only consider a single shift-invariance equation in each dimension. Therefore, unlike the partly calibrated stochastic CRB, where all sensor displacements  $\delta_i^x$  and  $\delta_i^y$  within each subarray are assumed to be known, only one sensor displacement in each dimension is utilized in the MD-Unitary-ESPRIT method. Thus, compared

(a) RMSE vs. SNR for  $N = 5$  snapshots

(b) RMSE vs. the number of snapshots for SNR = 0 dB

Fig. 4. Error performance for  $N_S = 2$  sources with correlation coefficient  $|\varphi| = 0.99$ , and spatial frequencies  $\boldsymbol{\mu}^x = [0.5, 0.8]^T$  and  $\boldsymbol{\mu}^y = [1.5, 1.2]^T$ .

to the previous scenario with uncorrelated sources in Fig. 3, for correlated sources, MD-Unitary-ESPRIT possesses a significant gap with respect to the partly calibrated CRB in the asymptotic region due to the lack of calibration information. On the other hand, SI-SPARROW outperforms MI-MD-ESPRIT and MD-Unitary-ESPRIT in both asymptotic and non-asymptotic regions, especially in difficult scenarios, e.g., in the case with low SNR and/or with a limited number of snapshots. Moreover, since the proposed MI-MD-ESPRIT method, which utilizes all the shift-invariance equations in (6b) and (6d) that involve the sensor displacements within each subarray, is performed on the solution of SI-SPARROW, the RMSE of SI-SPARROW asymptotically converges to the partly calibrated CRB. Nevertheless, SI-SPARROW exhibits an asymptotic bias with the increase of the number of snapshots due to the utilization of  $\ell_{2,1}$ -regularization.

Similar to the partly calibrated case, in the fully calibrated case, the MUSIC method performed on the solution of SI-SPARROW exhibits a significantly improved error performance and a considerably lower threshold, compared to MUSIC performed on the sample covariance matrix. However, compared to the previous uncorrelated scenario in Fig. 3, in Fig. 4, the SI-SPARROW method with MUSIC possesses a larger gap with respect to the fully calibrated CRB for high SNR and an asymptotic bias with the increase of the number of snapshots, due to the utilization of  $\ell_{2,1}$ -regularization. In

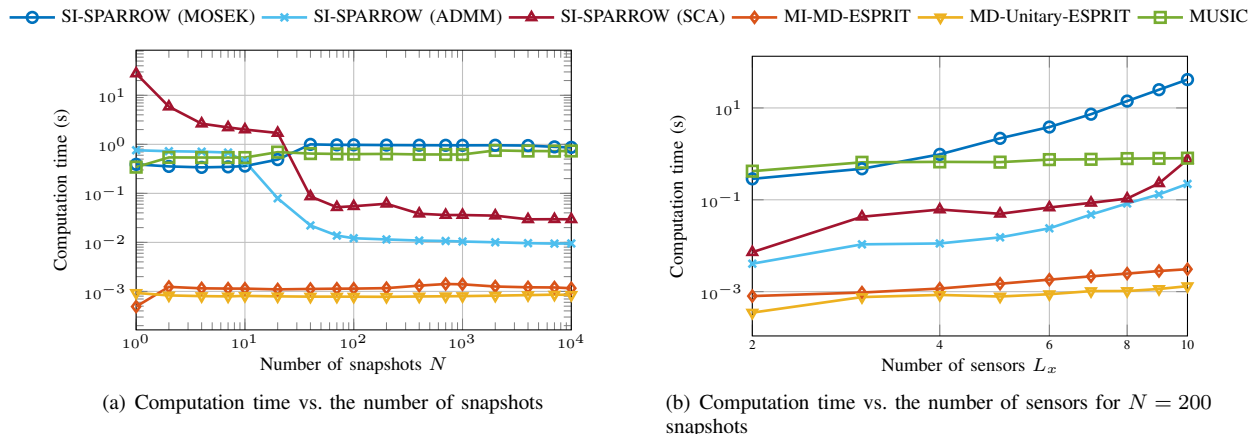


Fig. 5. Computation time for  $N_s = 2$  sources with correlation coefficient  $|\varphi| = 0.99$ , frequencies  $\boldsymbol{\mu}^x = [0.5, 0.8]^T$  and  $\boldsymbol{\mu}^y = [1.5, 1.2]^T$ , and SNR = 0 dB.

addition, similar to Fig. 3, it is observed in Fig. 4 that, when performed on the solution of SI-SPARROW, the fully calibrated MUSIC method is outperformed by the partly calibrated MI-MD-ESPRIT method in the region where the RMSE of MUSIC has not achieved the fully calibrated CRB.

### C. Computational Complexity

Next, we compare the computational costs of the different methods, in particular, the three solution approaches for the SI-SPARROW problem in (17), in Fig. 5 with varying the number of snapshots and the array size, respectively. In the three solution approaches for the SI-SPARROW problem, i.e., the SDP approach via the MOSEK solver, and the proposed ADMM Algorithm 1 and SCA Algorithm 3, suitable tolerances for the algorithm termination are selected so that they achieve similar precisions on the estimation quality. As discussed in Section II, to reduce the computational cost in the SDP implementation, the SDP reformulation (18) is employed in the undersampled case, whereas the equivalent SDP reformulation (19), whose constraint dimension is independent of the number of snapshots, is chosen in the oversampled case. We keep the scenario from the previous section with correlation coefficient  $\varphi = 0.99$ . The complexity of both MI-MD-ESPRIT and MD-Unitary-ESPRIT is dominated by the simultaneous diagonalization (or Schur decomposition). Specifically, both MI-MD-ESPRIT and MD-Unitary-ESPRIT admit closed-form solutions given the simultaneous diagonalization and, hence, they have the lowest computational cost compared to the two solutions approaches for SI-SPARROW. Also, it is observed in Fig. 5(a) that, as a typical property of subspace-based methods, the complexity of MI-MD-ESPRIT and MD-Unitary-ESPRIT is widely independent of the number of snapshots. In the undersampled case, the ADMM algorithm and the SDP implementation for SI-SPARROW exhibit similar computational costs, which are lower than those of the SCA algorithm. As analyzed in Section II, the complexity of the SDP reformulation in (18), which is used in the undersampled case, grows with the increase of the number of snapshots due to the increase of the dimension of the semidefinite matrix constraint, whereas in the oversampled case, due to the utilization of

the compact SDP reformulation in (19), the complexity of the SDP implementation remains constant with respect to the number of snapshots. In contrast, the complexity of both the ADMM algorithm and the SCA algorithm decreases dramatically with the increase of the number of snapshots since, in the oversampled case, the positive semidefiniteness constraint on  $\mathbf{Q}$  in (17) often becomes redundant and only the solution of the relaxed problem in (43) is required. In particular, both of them have a significantly lower computational cost than the SDP implementation in the oversampled case, and the ADMM algorithm has the lowest computational cost.

Then, in Fig. 5(b), we vary the array size in the oversampled case with  $N = 200$  snapshots by varying the number of sensors in each subarray in the  $x$ -axis  $L_x$  between 2 and 10, whereas the number of sensors in the  $y$ -axis  $L_y$  is fixed at 2. As shown in Fig. 5(b), the computational costs of both the SDP implementation and the ADMM algorithm for SI-SPARROW increase at similar rates with respect to the array size, which are higher than that of MI-MD-ESPRIT and MD-Unitary-ESPRIT. In addition, the complexity of MUSIC mainly depends on the grid size as a brute-force search over the grid is required and, therefore, the running time of MUSIC remains constant with respect to the variation of the number of snapshots and the array size in Fig. 5.

## VIII. CONCLUSION

In this paper, we consider the 2D DOA estimation problem from multiple measurement vectors (MMVs) using a partly calibrated rectangular array (PCRA). In particular, we employ a PCRA composed of identical subarrays where each subarray is fully calibrated but the intersubarray displacements are assumed to be unknown. Whereas the existing gridless methods are restricted to the case of uniform and fully calibrated array geometries, in this paper, we relax this requirement to shift-invariant partly calibrated arrays. We present a gridless sparsity-based method for the DOA estimation using the considered PCRA based on the shift-invariant SPARROW (SI-SPARROW) formulation proposed in [15] for the joint sparse reconstruction from MMVs with a partly calibrated linear array. Given the solution of the SI-SPARROW formulation,

a multidimensional ESPRIT-like method based on the simultaneous Schur decomposition [17] is then provided to finally recover and automatically pair the azimuth and elevation DOAs. Numerical simulations demonstrate the robustness of our proposed method to the source correlation, compared to the conventional partly calibrated DOA estimation methods, where the ESPRIT-like methods are performed on the sample covariance matrix. Moreover, in contrast to the SDP reformulation approach in [13] for the SPARROW problem, we develop two competitive algorithms under the ADMM and successive convex approximation (SCA) frameworks, respectively, for the established SI-SPARROW problem. Both proposed algorithms exhibit a significant reduction of the computation time with an increase of the number of snapshots in the numerical simulations, compared to the SDP implementation. In addition, since no calibration information is involved in the gridless SI-SPARROW formulation, this technique can also be used in the fully calibrated case to improve the robustness of subspace-based methods, e.g., MUSIC, to the source correlation. As shown in the simulations, compared to MUSIC performed on the sample covariance matrix, MUSIC performed on the solution of the SI-SPARROW formulation has considerably enhanced estimation quality for highly correlated sources.

#### APPENDIX A

##### FIRST- AND SECOND-ORDER TAYLOR EXPANSION OF $f$ IN (16)

In this section, we derive the gradient as well as the first- and second-order Taylor expansions of the function  $f$  in (16).

We remark that, in this paper, we only discuss the gradient of a real-valued function. The general definition of a gradient given in Section I is derived from the first-order Taylor expansion expressed with the Wirtinger derivatives. For a real-valued function  $f$  with complex-valued arguments  $\mathbf{x}$ , it holds that  $\left(\frac{\partial f}{\partial \mathbf{x}}\right)^* = \frac{\partial f}{\partial \mathbf{x}^*}$ . Therefore, the first-order Taylor expansion of  $f$  around a point  $\mathbf{x}^o$  is given by

$$\begin{aligned} f(\mathbf{x}) &\approx f(\mathbf{x}^o) + \left(\frac{\partial f(\mathbf{x}^o)}{\partial \mathbf{x}}\right)^\top (\mathbf{x} - \mathbf{x}^o) + \left(\frac{\partial f(\mathbf{x}^o)}{\partial \mathbf{x}^*}\right)^\top (\mathbf{x} - \mathbf{x}^o)^* \\ &= f(\mathbf{x}^o) + \Re \left( \left(2\frac{\partial f(\mathbf{x}^o)}{\partial \mathbf{x}^*}\right)^\text{H} (\mathbf{x} - \mathbf{x}^o) \right), \end{aligned}$$

which implies that the gradient of  $f$  at  $\mathbf{x}^o$  is

$$\nabla_{\mathbf{x}} f(\mathbf{x}^o) = 2\frac{\partial f(\mathbf{x}^o)}{\partial \mathbf{x}^*}. \quad (60)$$

However, the expression of gradient in (60) cannot be applied to the function  $f$  in (16) since the matrix  $\mathbf{Q}$  admits a Hermitian structure. Hence, to derive the gradient of  $f$  in (16) with respect to a Hermitian matrix  $\mathbf{Q}$ , we first establish the first-order Taylor expansion of  $f$ . For a general unstructured matrix  $\mathbf{Q} \in \mathbb{C}^{M \times M}$ , the function  $f$  is no longer real-valued and its Wirtinger derivatives are given by [40]

$$\begin{aligned} \frac{\partial f(\mathbf{Q})}{\partial \mathbf{Q}} &= -M[(\mathbf{Q} + \lambda \mathbf{I}_M)^{-1} \hat{\mathbf{R}}(\mathbf{Q} + \lambda \mathbf{I}_M)^{-1}]^\top + \mathbf{I}_M, \\ \text{and } \frac{\partial f(\mathbf{Q})}{\partial \mathbf{Q}^*} &= \mathbf{0}. \end{aligned} \quad (61)$$

With the above Wirtinger derivatives, the first-order Taylor expansion of  $f$  around a given point  $\mathbf{Q}^{(l)}$  can be written as

$$\begin{aligned} f(\mathbf{Q}) &\approx f(\mathbf{Q}^{(l)}) + \sum_{i=1}^M \sum_{j=1}^M \frac{\partial f(\mathbf{Q}^{(l)})}{\partial q_{i,j}} (q_{i,j} - q_{i,j}^{(l)}) \\ &= f(\mathbf{Q}^{(l)}) + \text{tr} \left( \left( \frac{\partial f(\mathbf{Q}^{(l)})}{\partial \mathbf{Q}} \right)^\top \Delta \right), \end{aligned} \quad (62)$$

where  $\Delta = \mathbf{Q} - \mathbf{Q}^{(l)}$ . When the matrix  $\mathbf{Q}$  is limited to be Hermitian, both terms in (62) become real-valued and the second term is the standard inner product of  $\left(\frac{\partial f(\mathbf{Q}^{(l)})}{\partial \mathbf{Q}}\right)^*$  and  $\Delta$  in the complex space. Hence, it can be identified that the gradient of  $f$  with respect to a Hermitian matrix  $\mathbf{Q}$  at  $\mathbf{Q}^{(l)}$  is

$$\begin{aligned} \nabla_{\mathbf{Q}} f(\mathbf{Q}^{(l)}) &= \left( \frac{\partial f(\mathbf{Q}^{(l)})}{\partial \mathbf{Q}} \right)^* \\ &= -M(\mathbf{Q}^{(l)} + \lambda \mathbf{I}_M)^{-1} \hat{\mathbf{R}}(\mathbf{Q}^{(l)} + \lambda \mathbf{I}_M)^{-1} + \mathbf{I}_M. \end{aligned} \quad (63)$$

Then, following the same procedure as in [29, Appendix A.4.3], we can obtain the second-order Taylor expansion of  $f$  in (17) around a given point  $\mathbf{Q}^{(l)}$  by first deriving the first-order Taylor expansion of its gradient. For a point  $\mathbf{Q}$  near  $\mathbf{Q}^{(l)}$ , define  $\Delta = \mathbf{Q} - \mathbf{Q}^{(l)}$  and  $\mathbf{W} = \mathbf{Q}^{(l)} + \lambda \mathbf{I}_M$ . For the gradient  $\nabla_{\mathbf{Q}} f$  given in (63), its first-order Taylor expansion around  $\mathbf{Q}^{(l)}$  can be expressed in (64) by using the first-order approximation  $(\mathbf{I} + \mathbf{A})^{-1} \approx \mathbf{I} - \mathbf{A}$  for  $\|\mathbf{A}\|_F$  being small. Then the second-order Taylor expansion of  $f$  in (16) can be obtained by integrating the first-order Taylor expansion of its gradient, which leads to the following expression:

$$\begin{aligned} f(\mathbf{Q}) &\approx f(\mathbf{Q}^{(l)}) + \text{tr}(\nabla_{\mathbf{Q}} f(\mathbf{Q}^{(l)}) \Delta) \\ &\quad + \frac{M}{2} \text{tr}((\mathbf{V} \Delta \tilde{\mathbf{R}} + \tilde{\mathbf{R}} \Delta \mathbf{V}) \Delta) \\ &= f(\mathbf{Q}^{(l)}) + \text{tr}(\nabla_{\mathbf{Q}} f(\mathbf{Q}^{(l)}) \Delta) + M \text{tr}(\mathbf{V} \Delta \tilde{\mathbf{R}} \Delta) \end{aligned} \quad (65)$$

with  $\mathbf{V} = \mathbf{W}^{-1} = (\mathbf{Q}^{(l)} + \lambda \mathbf{I}_M)^{-1}$  and  $\tilde{\mathbf{R}} = \mathbf{V} \hat{\mathbf{R}} \mathbf{V}$ . The last inequality in (65) comes from the cyclic property of trace.

#### APPENDIX B

##### STOCHASTIC CRAMÉR-RAO BOUND FOR PCRAS

In this section, we provide the details of the calculation of the stochastic Cramér-Rao Bound (CRB) for the estimation of the spatial frequencies  $\boldsymbol{\mu}$  in PCRAs under the signal model given in (2), by following a line of analysis similar to that in [9] for linear PCAs. For simplicity, the steering matrix  $\mathbf{A}(\boldsymbol{\mu})$  in (2) is denoted by  $\mathbf{A}$  in this section.

Consider the signal model in (2). The stochastic model, also referred to as the unconditional model assumption (UMA) [39], [41], assumes that the source waveforms  $\boldsymbol{\Psi}$  are stochastic. Specifically, the waveform vector  $\boldsymbol{\psi}_n$  at each time instant i.i.d. follows the Gaussian distribution

$$\boldsymbol{\psi}_n \sim \mathcal{CN}(\mathbf{0}, \mathbf{P}), \quad (66)$$

where  $\mathbf{P} \in \mathbb{C}^{N_S \times N_S}$  is the unknown source covariance matrix. Then, each snapshot  $\mathbf{y}_n$  i.i.d. follows the Gaussian distribution

$$\mathbf{y}_n \sim \mathcal{CN}(\mathbf{0}, \mathbf{R}) \quad \text{with } \mathbf{R} = \mathbf{A} \mathbf{P} \mathbf{A}^\text{H} + \sigma_n^2 \mathbf{I}_M. \quad (67)$$

To derive the CRB, we first introduce the following decomposition of the steering vectors. The components  $\mathbf{a}_x(\mu^x)$  and  $\mathbf{a}_y(\mu^y)$  in (4) for a given direction  $(\mu^x, \mu^y)$  can be expressed as the Kronecker products

$$\mathbf{a}^x(\mu^x) = \mathbf{h}^x(\mu^x, \boldsymbol{\alpha}^x) \otimes \mathbf{v}^x(\mu^x), \quad (68a)$$

$$\mathbf{a}^y(\mu^y) = \mathbf{h}^y(\mu^y, \boldsymbol{\alpha}^y) \otimes \mathbf{v}^y(\mu^y), \quad (68b)$$

where the vectors  $\mathbf{v}^x(\mu^x) \in \mathbb{C}^{L_x}$  and  $\mathbf{v}^y(\mu^y) \in \mathbb{C}^{L_y}$  characterize the nominal array response vectors, i.e., the calibrated part of the array manifold, in the two dimensions, respectively. They are defined in (23) with the known intrasubarray displacements. On the other hand, the vectors  $\mathbf{h}^x(\mu^x, \boldsymbol{\alpha}^x) \in \mathbb{C}^{P_x}$  and  $\mathbf{h}^y(\mu^y, \boldsymbol{\alpha}^y) \in \mathbb{C}^{P_y}$  characterize the unknown perturbations of the nominal array response, i.e., the uncalibrated part of the array manifold, which depend on not only the frequencies  $(\mu^x, \mu^y)$  but also the unknown array parameters that are summarized in the vectors  $\boldsymbol{\alpha}^x$  and  $\boldsymbol{\alpha}^y$  for the two dimensions, respectively. For the PCRA depicted in Fig. 1,  $\boldsymbol{\alpha}^x$  and  $\boldsymbol{\alpha}^y$  contain the unknown intersubarray displacements  $\Delta_2^x, \dots, \Delta_{P_x}^x$  and  $\Delta_2^y, \dots, \Delta_{P_y}^y$  in the two dimensions, respectively, and the vectors  $\mathbf{h}^x$  and  $\mathbf{h}^y$  can be expressed as

$$\mathbf{h}^x(\mu^x, \boldsymbol{\alpha}^x) = [1, e^{j\mu^x \Delta_2^x}, \dots, e^{j\mu^x \Delta_{P_x}^x}]^T, \quad (69a)$$

$$\mathbf{h}^y(\mu^y, \boldsymbol{\alpha}^y) = [1, e^{j\mu^y \Delta_2^y}, \dots, e^{j\mu^y \Delta_{P_y}^y}]^T. \quad (69b)$$

To simplify the calculation of the CRB, we ignore the relations in (69) and directly consider the entries of the vectors  $\mathbf{h}^x$  and  $\mathbf{h}^y$  as the parameters to be recovered. For simplicity, we denote  $\mathbf{h}^x(\mu_i^x, \boldsymbol{\alpha}^x)$  and  $\mathbf{h}^y(\mu_i^y, \boldsymbol{\alpha}^y)$  as  $\mathbf{h}_i^x = [h_{1,i}^x, \dots, h_{P_x,i}^x]^T$  and  $\mathbf{h}_i^y = [h_{1,i}^y, \dots, h_{P_y,i}^y]^T$ . Note that, due to the decomposition in (68), each vector  $\mathbf{h}_i^x$  or  $\mathbf{h}_i^y$  is only identifiable up to a scaling constant. To avoid such a scaling ambiguity in the calculation of the CRB, the first entries of the vectors  $\mathbf{h}_i^x$  and  $\mathbf{h}_i^y$  are considered to be known and fixed at 1. Thus, we summarize those unknown parameters in the following real-valued  $2N_S(P_x + P_y - 1) \times 1$  vector:

$$\boldsymbol{\eta} = [(\mu^x)^T, (\mu^y)^T, (\boldsymbol{\xi}_2^x)^T, \dots, (\boldsymbol{\xi}_{P_x}^x)^T, (\boldsymbol{\zeta}_2^x)^T, \dots, (\boldsymbol{\zeta}_{P_x}^x)^T, (\boldsymbol{\xi}_2^y)^T, \dots, (\boldsymbol{\xi}_{P_y}^y)^T, (\boldsymbol{\zeta}_2^y)^T, \dots, \boldsymbol{\zeta}^y]^T, \quad (70)$$

where

$$\begin{aligned} \boldsymbol{\xi}_p^x &= [\Re(h_{p,1}^x), \dots, \Re(h_{p,N_S}^x)]^T \quad \text{and} \\ \boldsymbol{\zeta}_p^x &= [\Im(h_{p,1}^x), \dots, \Im(h_{p,N_S}^x)]^T \quad \text{for } p = 2, \dots, P_x, \end{aligned} \quad (71)$$

$$\begin{aligned} \boldsymbol{\xi}_p^y &= [\Re(h_{p,1}^y), \dots, \Re(h_{p,N_S}^y)]^T \quad \text{and} \\ \boldsymbol{\zeta}_p^y &= [\Im(h_{p,1}^y), \dots, \Im(h_{p,N_S}^y)]^T \quad \text{for } p = 2, \dots, P_y. \end{aligned} \quad (72)$$

Under the UMA model in (67), the unknown parameters of the problem include the entries of the vector  $\boldsymbol{\eta}$ , the noise variance  $\sigma_n^2$ , and the entries of the source covariance matrix  $\mathbf{P}$ . However, as shown in [39], [41], only the parameters in the vector  $\boldsymbol{\eta}$  are involved in the calculation of the block of the CRB matrix corresponding to the spatial frequencies  $\boldsymbol{\mu}$ , which we are interested in. By concentrating the problem with respect

to the nuisance parameters, i.e., the noise variances  $\sigma_n^2$  and the source covariance matrix  $\mathbf{P}$ , the entries of the inverse of the  $2N_S(P_x + P_y - 1) \times 2N_S(P_x + P_y - 1)$   $\boldsymbol{\eta}$ -block of the CRB matrix, denoted by  $\text{CRB}(\boldsymbol{\eta})$ , can be expressed as

$$[\text{CRB}^{-1}(\boldsymbol{\eta})]_{k,l} = \frac{2N}{\sigma_n^2} \Re \left( \text{tr} \left( \mathbf{U} \frac{\partial \mathbf{A}^H}{\partial \eta_k} \boldsymbol{\Pi}_A^\perp \frac{\partial \mathbf{A}}{\partial \eta_l} \right) \right), \quad (73)$$

where  $\boldsymbol{\Pi}_A^\perp = \mathbf{I} - \mathbf{A}(\mathbf{A}^H \mathbf{A})^{-1} \mathbf{A}^H$  is the orthogonal projector onto the orthogonal complement of the column space of the steering matrix  $\mathbf{A}$  and

$$\mathbf{U} = \mathbf{P} \mathbf{A}^H \mathbf{R}^{-1} \mathbf{A} \mathbf{P} = \mathbf{P} (\mathbf{A}^H \mathbf{A} \mathbf{P} + \sigma_n^2 \mathbf{I})^{-1} \mathbf{A}^H \mathbf{A} \mathbf{P}. \quad (74)$$

Omitting the intermediate calculations from (73), we can write the  $\boldsymbol{\eta}$ -block of the CRB matrix in a compact form as

$$\text{CRB}(\boldsymbol{\eta}) = \frac{\sigma_n^2}{2N} [\Re((\mathbf{D}^H \boldsymbol{\Pi}_A^\perp \mathbf{D}) \odot (\mathbf{1} \mathbf{1}^T \otimes \mathbf{U}^T))]^{-1}, \quad (75)$$

where

$$\begin{aligned} \mathbf{D} &= [\mathbf{D}_{\mu^x}, \mathbf{D}_{\mu^y}, \mathbf{D}_{\boldsymbol{\xi}_2^x}, \dots, \mathbf{D}_{\boldsymbol{\xi}_{P_x}^x}, \mathbf{D}_{\boldsymbol{\zeta}_2^x}, \dots, \mathbf{D}_{\boldsymbol{\zeta}_{P_x}^x}, \\ &\quad \mathbf{D}_{\boldsymbol{\xi}_2^y}, \dots, \mathbf{D}_{\boldsymbol{\xi}_{P_y}^y}, \mathbf{D}_{\boldsymbol{\zeta}_2^y}, \dots, \mathbf{D}_{\boldsymbol{\zeta}_{P_y}^y}], \end{aligned} \quad (76)$$

$$\mathbf{D}_{\mu^x} = \left[ \frac{\partial \mathbf{a}(\mu_1^x, \mu_1^y)}{\partial \mu_1^x}, \dots, \frac{\partial \mathbf{a}(\mu_{N_S}^x, \mu_{N_S}^y)}{\partial \mu_{N_S}^x} \right], \quad (77)$$

$$\mathbf{D}_{\mu^y} = \left[ \frac{\partial \mathbf{a}(\mu_1^x, \mu_1^y)}{\partial \mu_1^y}, \dots, \frac{\partial \mathbf{a}(\mu_{N_S}^x, \mu_{N_S}^y)}{\partial \mu_{N_S}^y} \right], \quad (78)$$

$$\mathbf{D}_{\boldsymbol{\xi}_p^x} = \left[ \frac{\partial \mathbf{a}(\mu_1^x, \mu_1^y)}{\partial \xi_{1,p}^x}, \dots, \frac{\partial \mathbf{a}(\mu_{N_S}^x, \mu_{N_S}^y)}{\partial \xi_{N_S,p}^x} \right] \quad \text{and}$$

$$\begin{aligned} \mathbf{D}_{\boldsymbol{\zeta}_p^x} &= \left[ \frac{\partial \mathbf{a}(\mu_1^x, \mu_1^y)}{\partial \zeta_{1,p}^x}, \dots, \frac{\partial \mathbf{a}(\mu_{N_S}^x, \mu_{N_S}^y)}{\partial \zeta_{N_S,p}^x} \right] = j \mathbf{D}_{\boldsymbol{\xi}_p^x} \\ &\quad \text{for } p = 2, \dots, P_x, \end{aligned} \quad (79)$$

$$\mathbf{D}_{\boldsymbol{\xi}_p^y} = \left[ \frac{\partial \mathbf{a}(\mu_1^x, \mu_1^y)}{\partial \xi_{1,p}^y}, \dots, \frac{\partial \mathbf{a}(\mu_{N_S}^x, \mu_{N_S}^y)}{\partial \xi_{N_S,p}^y} \right] \quad \text{and}$$

$$\begin{aligned} \mathbf{D}_{\boldsymbol{\zeta}_p^y} &= \left[ \frac{\partial \mathbf{a}(\mu_1^x, \mu_1^y)}{\partial \zeta_{1,p}^y}, \dots, \frac{\partial \mathbf{a}(\mu_{N_S}^x, \mu_{N_S}^y)}{\partial \zeta_{N_S,p}^y} \right] = j \mathbf{D}_{\boldsymbol{\xi}_p^y} \\ &\quad \text{for } p = 2, \dots, P_y. \end{aligned} \quad (80)$$

According to the model in (68), the derivatives can be calculated as in (81). The square root of the average of the diagonal entries corresponding to the spatial frequencies  $\boldsymbol{\mu}$  in the CRB matrix provides a lower bound for the RMSE in the estimation of  $\boldsymbol{\mu}$  and it is, therefore, used as a reference for the estimation performance evaluation in Section VII.

## REFERENCES

- [1] R. Schmidt, "Multiple emitter location and signal parameter estimation," *IEEE Trans. Antennas Propag.*, vol. 34, no. 3, pp. 276–280, Mar. 1986.

$$\begin{aligned} \nabla_Q f(Q) &= -M(\mathbf{W} + \boldsymbol{\Delta})^{-1} \cdot \widehat{\mathbf{R}} \cdot (\mathbf{W} + \boldsymbol{\Delta})^{-1} + \mathbf{I}_M \\ &= -M \mathbf{W}^{-\frac{1}{2}} \left( \mathbf{I}_M + \mathbf{W}^{-\frac{1}{2}} \boldsymbol{\Delta} \mathbf{W}^{-\frac{1}{2}} \right)^{-1} \mathbf{W}^{-\frac{1}{2}} \cdot \widehat{\mathbf{R}} \cdot \mathbf{W}^{-\frac{1}{2}} \left( \mathbf{I}_M + \mathbf{W}^{-\frac{1}{2}} \boldsymbol{\Delta} \mathbf{W}^{-\frac{1}{2}} \right)^{-1} \mathbf{W}^{-\frac{1}{2}} + \mathbf{I}_M \\ &\approx -M \mathbf{W}^{-\frac{1}{2}} \left( \mathbf{I}_M - \mathbf{W}^{-\frac{1}{2}} \boldsymbol{\Delta} \mathbf{W}^{-\frac{1}{2}} \right) \mathbf{W}^{-\frac{1}{2}} \cdot \widehat{\mathbf{R}} \cdot \mathbf{W}^{-\frac{1}{2}} \left( \mathbf{I}_M - \mathbf{W}^{-\frac{1}{2}} \boldsymbol{\Delta} \mathbf{W}^{-\frac{1}{2}} \right) \mathbf{W}^{-\frac{1}{2}} + \mathbf{I}_M \\ &= -M (\mathbf{W}^{-1} - \mathbf{W}^{-1} \boldsymbol{\Delta} \mathbf{W}^{-1}) \cdot \widehat{\mathbf{R}} \cdot (\mathbf{W}^{-1} - \mathbf{W}^{-1} \boldsymbol{\Delta} \mathbf{W}^{-1}) + \mathbf{I}_M \\ &= \underbrace{-M \mathbf{W}^{-1} \widehat{\mathbf{R}} \mathbf{W}^{-1} + \mathbf{I}_M}_{\nabla_Q f(Q^{(l)})} + M(\mathbf{W}^{-1} \boldsymbol{\Delta} \mathbf{W}^{-1} \widehat{\mathbf{R}} \mathbf{W}^{-1} + \mathbf{W}^{-1} \widehat{\mathbf{R}} \mathbf{W}^{-1} \boldsymbol{\Delta} \mathbf{W}^{-1}) - \underbrace{M \mathbf{W}^{-1} \boldsymbol{\Delta} \mathbf{W}^{-1} \widehat{\mathbf{R}} \mathbf{W}^{-1} \boldsymbol{\Delta} \mathbf{W}^{-1}}_{o(\|\boldsymbol{\Delta}\|_F)} \\ &\approx \nabla_Q f(Q^{(l)}) + M(\mathbf{W}^{-1} \boldsymbol{\Delta} \mathbf{W}^{-1} \widehat{\mathbf{R}} \mathbf{W}^{-1} + \mathbf{W}^{-1} \widehat{\mathbf{R}} \mathbf{W}^{-1} \boldsymbol{\Delta} \mathbf{W}^{-1}) \end{aligned} \quad (64)$$

- [2] R. Roy and T. Kailath, "ESPRIT-estimation of signal parameters via rotational invariance techniques," *IEEE Trans. Acoust. Speech Signal Process.*, vol. 37, no. 7, pp. 984–995, Jul. 1989.
- [3] M. Haardt and J. A. Nosske, "Unitary ESPRIT: how to obtain increased estimation accuracy with a reduced computational burden," *IEEE Trans. Signal Process.*, vol. 43, no. 5, pp. 1232–1242, May 1995.
- [4] B. Friedlander, "A sensitivity analysis of the MUSIC algorithm," *IEEE Trans. Acoust. Speech Signal Process.*, vol. 38, no. 10, pp. 1740–1751, Oct. 1990.
- [5] B. C. Ng and W. Ser, "Array shape calibration using sources in known locations," in *Proc. Singap. ICCSISITA 92*, 1992, pp. 836–840 vol.2.
- [6] B. Liao and S. C. Chan, "A review on direction finding in partly calibrated arrays," in *2014 19th Int. Conf. Digit. Signal Process.*, Aug. 2014, pp. 812–816.
- [7] M. Pesavento, A. B. Gershman, and K. M. Wong, "Direction finding in partly calibrated sensor arrays composed of multiple subarrays," *IEEE Trans. Signal Process.*, vol. 50, no. 9, pp. 2103–2115, Sep. 2002.
- [8] P. Parvazi, M. Pesavento, and A. B. Gershman, "Direction-of-arrival estimation and array calibration for partly-calibrated arrays," in *2011 IEEE Int. Conf. Acoust. Speech Signal Process. ICASSP*, May 2011, pp. 2552–2555.
- [9] C. M. S. See and A. B. Gershman, "Direction-of-arrival estimation in partly calibrated subarray-based sensor arrays," *IEEE Trans. Signal Process.*, vol. 52, no. 2, pp. 329–338, Feb. 2004.
- [10] M. Pesavento, A. Gershman, and K. M. Wong, "Direction of arrival estimation in partly calibrated time-varying sensor arrays," in *2001 IEEE Int. Conf. Acoust. Speech Signal Process. Proc. Cat No01CH37221*, vol. 5, May 2001, pp. 3005–3008 vol.5.
- [11] P. Parvazi and M. Pesavento, "A new direction-of-arrival estimation and calibration method for arrays composed of multiple identical subarrays," in *2011 IEEE 12th Int. Workshop Signal Process. Adv. Wirel. Commun.*, Jun. 2011, pp. 171–175.
- [12] C. Steffens, P. Parvazi, and M. Pesavento, "Direction finding and array calibration based on sparse reconstruction in partly calibrated arrays," in *2014 IEEE 8th Sens. Array Multichannel Signal Process. Workshop SAM*, Jun. 2014, pp. 21–24.
- [13] C. Steffens, M. Pesavento, and M. E. Pfetsch, "A compact formulation for the  $\ell_{2,1}$  mixed-norm minimization problem," *IEEE Trans. Signal Process.*, vol. 66, no. 6, pp. 1483–1497, Mar. 2018.
- [14] C. Steffens and M. Pesavento, "Block- and rank-sparse recovery for direction finding in partly calibrated arrays," *IEEE Trans. Signal Process.*, vol. 66, no. 2, pp. 384–399, Jan. 2018.
- [15] C. Steffens, W. Suleiman, A. Sorg, and M. Pesavento, "Gridless compressed sensing under shift-invariant sampling," in *2017 IEEE Int. Conf. Acoust. Speech Signal Process. ICASSP*, Mar. 2017, pp. 4735–4739.
- [16] G. Zhang, T. Huang, Y. Liu, X. Wang, and Y. C. Eldar, "Direction finding in partly calibrated arrays exploiting the whole array aperture," Dec. 2022.
- [17] M. Haardt and J. A. Nosske, "Simultaneous Schur decomposition of several nonsymmetric matrices to achieve automatic pairing in multidimensional harmonic retrieval problems," *IEEE Trans. Signal Process.*, vol. 46, no. 1, pp. 161–169, 1998.
- [18] M. R. Spiegel, S. Lipschutz, J. J. Schiller, and D. Spellman, *Complex variables*, 2nd ed. The McGraw-Hill Companies, 2009.
- [19] J. Zhang and M. Haardt, "Channel estimation and training design for hybrid multi-carrier mmWave massive MIMO systems: The beamspace ESPRIT approach," in *2017 25th Eur. Signal Process. Conf. EUSIPCO*, 2017, pp. 385–389.
- [20] M. D. Zoltowski, M. Haardt, and C. P. Mathews, "Closed-form 2-D angle estimation with rectangular arrays in element space or beamspace via unitary ESPRIT," *IEEE Trans. Signal Process.*, vol. 44, no. 2, pp. 316–328, Feb. 1996.
- [21] MOSEK ApS, "The MOSEK optimization toolbox for MATLAB. Version 10.0.22." <https://docs.mosek.com/10.0.22/toolbox/index.html>.
- [22] Y. Chi, L. L. Scharf, A. Pezeshki, and A. R. Calderbank, "Sensitivity to basis mismatch in compressed sensing," *IEEE Trans. Signal Process.*, vol. 59, no. 5, pp. 2182–2195, May 2011.
- [23] M. A. Herman and T. Strohmer, "General deviants: an analysis of perturbations in compressed sensing," *IEEE J. Sel. Top. Signal Process.*, vol. 4, no. 2, pp. 342–349, Apr. 2010.
- [24] E. J. Candès and B. Recht, "Exact matrix completion via convex optimization," *Found Comput Math*, vol. 9, no. 6, pp. 717–772, Dec. 2009.
- [25] Z. Yang, L. Xie, and P. Stoica, "Vandermonde decomposition of multilevel toeplitz matrices with application to multidimensional super-resolution," *IEEE Trans. Inf. Theory*, vol. 62, no. 6, pp. 3685–3701, Jun. 2016.
- [26] T. Fu and X. Gao, "Simultaneous diagonalization with similarity transformation for non-defective matrices," in *2006 IEEE Int. Conf. Acoust. Speech Signal Process.*, vol. 4, May 2006, pp. IV–IV.
- [27] S. Boyd, N. Parikh, E. Chu, B. Peleato, and J. Eckstein, "Distributed optimization and statistical learning via the alternating direction method of multipliers," *Found. Trends Mach. Learn.*, vol. 3, no. 1, pp. 1–122, 2011.
- [28] N. J. Higham, "Computing a nearest symmetric positive semidefinite matrix," *Linear Algebra and its Applications*, vol. 103, pp. 103–118, May 1988.
- [29] S. Boyd and L. Vandenberghe, *Convex optimization*. Cambridge University Press, 2004.
- [30] Y. Yang and M. Pesavento, "A unified successive pseudoconvex approximation framework," *IEEE Trans. Signal Process.*, vol. 65, no. 13, pp. 3313–3328, 2017.
- [31] D. P. Bertsekas, *Nonlinear programming*, 3rd ed. Belmont, Mass: Athena scientific, 2016.
- [32] B. S. He, H. Yang, and S. L. Wang, "Alternating direction method with self-adaptive penalty parameters for monotone variational inequalities," *Journal of Optimization Theory and Applications*, vol. 106, no. 2, pp. 337–356, Aug. 2000.
- [33] S. L. Wang and L. Z. Liao, "Decomposition method with a variable parameter for a class of monotone variational inequality problems," *Journal of Optimization Theory and Applications*, vol. 109, no. 2, pp. 415–429, May 2001.
- [34] T. J. Suffridge and T. L. Hayden, "Approximation by a Hermitian positive semidefinite Toeplitz matrix," *SIAM J. Matrix Anal. Appl.*, vol. 14, no. 3, pp. 721–734, Jul. 1993.
- [35] R. L. Dykstra, "An algorithm for restricted least squares regression," *J. Am. Stat. Assoc.*, vol. 78, no. 384, pp. 837–842, 1983.
- [36] H. H. Bauschke and J. M. Borwein, "Dykstra's alternating projection algorithm for two sets," *Journal of Approximation Theory*, vol. 79, no. 3, pp. 418–443, Dec. 1994.
- [37] M. C. Grant and S. P. Boyd, "CVX: matlab software for disciplined convex programming, version 2.2," <http://cvxr.com/cvx/>, Jan. 2020.

$$\frac{\partial \mathbf{a}(\mu_i^x, \mu_i^y)}{\partial \mu_i^x} = \frac{\partial \mathbf{a}^x(\mu_i^x)}{\partial \mu_i^x} \otimes \mathbf{a}^y(\mu_i^y) = \mathbf{h}_i^x \otimes \frac{\partial \mathbf{v}^x(\mu_i^x)}{\partial \mu_i^x} \otimes \mathbf{a}^y(\mu_i^y)$$

$$\text{with } \frac{\partial \mathbf{v}^x(\mu_i^x)}{\partial \mu_i^x} = [\mathbf{j}\delta_1^x e^{j\mu_i^x \delta_1^x} \quad \dots \quad \mathbf{j}\delta_{L_x}^x e^{j\mu_i^x \delta_{L_x}^x}]^T \text{ for } i = 1, \dots, N_S, \quad (81a)$$

$$\frac{\partial \mathbf{a}(\mu_i^x, \mu_i^y)}{\partial \mu_i^y} = \mathbf{a}^x(\mu_i^x) \otimes \frac{\partial \mathbf{a}^y(\mu_i^y)}{\partial \mu_i^y} = \mathbf{a}^x(\mu_i^x) \otimes \mathbf{h}_i^y \otimes \frac{\partial \mathbf{v}^y(\mu_i^y)}{\partial \mu_i^y}$$

$$\text{with } \frac{\partial \mathbf{v}^y(\mu_i^y)}{\partial \mu_i^y} = [\mathbf{j}\delta_1^y e^{j\mu_i^y \delta_1^y} \quad \dots \quad \mathbf{j}\delta_{L_y}^y e^{j\mu_i^y \delta_{L_y}^y}]^T \text{ for } i = 1, \dots, N_S, \quad (81b)$$

$$\frac{\partial \mathbf{a}(\mu_i^x, \mu_i^y)}{\partial \xi_{i,p}^x} = \frac{\mathbf{a}^x(\mu_i^x)}{\partial \xi_{i,p}^x} \otimes \mathbf{a}^y(\mu_i^y) = \frac{\partial \mathbf{h}_i^x}{\partial \xi_{i,p}^x} \otimes \mathbf{v}^x(\mu_i^x) \otimes \mathbf{a}^y(\mu_i^y) = \mathbf{e}_{P_x,p} \otimes \mathbf{v}^x(\mu_i^x) \otimes \mathbf{a}^y(\mu_i^y)$$

$$\text{for } i = 1, \dots, N_S \text{ and } p = 1, \dots, P_x, \quad (81c)$$

$$\frac{\partial \mathbf{a}(\mu_i^x, \mu_i^y)}{\partial \xi_{i,p}^y} = \mathbf{a}^x(\mu_i^x) \otimes \frac{\partial \mathbf{a}^y(\mu_i^y)}{\partial \xi_{i,p}^y} = \mathbf{a}^x(\mu_i^x) \otimes \frac{\partial \mathbf{h}_i^y}{\partial \xi_{i,p}^y} \otimes \mathbf{v}^y(\mu_i^y) = \mathbf{a}^x(\mu_i^x) \otimes \mathbf{e}_{P_y,p} \otimes \mathbf{v}^y(\mu_i^y)$$

$$\text{for } i = 1, \dots, N_S \text{ and } p = 1, \dots, P_y \quad (81d)$$

- [38] ———, “Graph implementations for nonsmooth convex programs,” in *Recent Adv. Learn. Control*, ser. Lecture Notes in Control and Information Sciences, V. D. Blondel, S. P. Boyd, and H. Kimura, Eds. London: Springer, 2008, pp. 95–110.
- [39] P. Stoica, E. G. Larsson, and A. B. Gershman, “The stochastic CRB for array processing: a textbook derivation,” *IEEE Signal Process. Lett.*, vol. 8, no. 5, pp. 148–150, May 2001.
- [40] A. Hjørungnes and D. Gesbert, “Complex-Valued Matrix Differentiation: Techniques and Key Results,” *IEEE Trans. Signal Process.*, vol. 55, no. 6, pp. 2740–2746, 2007.
- [41] P. Stoica and A. Nehorai, “Performance study of conditional and unconditional direction-of-arrival estimation,” *IEEE Trans. Acoust. Speech Signal Process.*, vol. 38, no. 10, pp. 1783–1795, Oct. 1990.